



Mesoporous silica-supported lipid bilayers (protocells) for DNA cargo delivery to the spinal cord



Ellen C. Dengler^a, Juewen Liu^b, Audra Kerwin^a, Sergio Torres^a, Clara M. Olcott^a, Brandi N. Bowman^a, Leisha Armijo^a, Katherine Gentry^c, Jenny Wilkerson^a, James Wallace^a, Xingmao Jiang^b, Eric C. Carnes^b, C. Jeffrey Brinker^b, Erin D. Milligan^{d,*}

^a Department of Neurosciences, Health Sciences Center, University of New Mexico, Albuquerque, NM, USA

^b Department of Chemical and Nuclear Engineering, University of New Mexico, Albuquerque, NM, USA

^c Department of Anesthesiology and Critical Care Medicine, Health Sciences Center, University of New Mexico, Albuquerque, NM, USA

^d Department of Neurosciences, Health Sciences Center, School of Medicine, University of New Mexico, Albuquerque, NM 87131-5223, USA

ARTICLE INFO

Article history:

Received 8 June 2012

Accepted 8 March 2013

Available online 18 March 2013

Keywords:

Interleukin-10 cytokine

Gene delivery

Biocompatibility

Neuropathic pain

Cell and tissue viability

Non-viral vector

ABSTRACT

Amorphous mesoporous silica nanoparticles ('protocells') that support surface lipid bilayers recently characterized *in vitro* as carrier constructs for small drug and DNA delivery are reported here as highly biocompatible both *in vitro* and *in vivo*, involving the brain and spinal cord following spinal delivery into the lumbosacral subarachnoid space (intrathecal; i.t.). Specifically, positively charged, 1, 2-Dioleoyl-3-Trimethylammonium-Propane (DOTAP)-cholesterol (DOTAP:Chol) liposome-formulated protocells revealed stable *in vitro* cargo release kinetics and cellular interleukin-10 (IL-10) transgene transfection. Recent approaches using synthetic non-viral vector platforms to deliver the pain-suppressive therapeutic transgene, IL-10, to the spinal subarachnoid space have yielded promising results in animal models of peripheral neuropathy, a condition involving aberrant neuronal communication within sensory pathways in the nervous system.

Non-viral drug and gene delivery protocell platforms offer potential flexibility because cargo release-rates can be pH-dependent. We report here that i.t. delivery of protocells, with modified chemistry supporting a surface coating of DOTAP:Chol liposomes and containing the IL-10 transgene, results in functional suppression of pain-related behavior in rats for extended periods. This study is the first demonstration that protocell vectors offer amenable and enduring *in vivo* biological characteristics that can be applied to spinal gene delivery.

© 2013 Elsevier B.V. Open access under [CC BY-NC-ND license](http://creativecommons.org/licenses/by-nc-nd/3.0/).

1. Introduction

The development of synthetic non-viral vectors for gene therapeutic purposes has steadily increased during the past 10 years, an effort that is reflected by increased non-viral gene therapeutic clinical trials worldwide [1,2]. While viral vectors are superior in gene transfection efficiency, non-viral gene transfer systems are associated with less safety concerns. The application of central nervous system (CNS) non-viral gene transfer to express therapeutic proteins is significantly underexplored in light of the broad-ranging therapeutic potential in controlling a host of neurological diseases. The arsenal of potential clinical gene delivery platforms includes cationic lipids and peptides,

co-polymers, polymeric micelles, and modified silica nanoparticles [3–5]. Indeed, a significant amount of progress toward our understanding and utilizing mesoporous silica nanoparticles (MSN) for controlled drug and gene release, while optimizing biocompatibility, has occurred in recent years [6]. Silicas are present in crystalline and non-crystalline (amorphous) forms, with amorphous silica occurring either naturally or are synthesized. While crystalline silica is widely associated with adverse health effects including silicosis that involves proinflammatory cytokine-mediated pathogenesis, virtually no toxicity has been identified with synthetic amorphous silicas at moderate doses [7,8]. Therefore, synthetic amorphous silicas have been explored in biomedical applications including targeted drug delivery for cancer chemotherapeutics and DNA delivery for gene therapy [9,10]. The major advantage of using synthesized MSNs is that their surface can be chemically modified resulting in improvements in their drug cargo capacity as well as facilitation of tunable release rates which further enhances their biocompatibility and functional capabilities [11].

Mesoporous silicas contain a porous structure with hundreds of channels referred to as mesopores, which are able to adsorb bioactive

* Corresponding author. Tel.: +1 505 272 8103; fax: +1 505 272 8082.

E-mail addresses: edengler@salud.unm.edu (E.C. Dengler), liujuewen@gmail.com (J. Liu), akerwin@salud.unm.edu (A. Kerwin), sertorres@salud.unm.edu (S. Torres), colcott@salud.unm.edu (C.M. Olcott), bbowman@salud.unm.edu (B.N. Bowman), liesha.armijo@gmail.com (L. Armijo), k8gentry@gmail.com (K. Gentry), jlwilkerson@salud.unm.edu (J. Wilkerson), jwallace@salud.unm.edu (J. Wallace), jiangxm@unm.edu (X. Jiang), eric.carnes@gmail.com (E.C. Carnes), cjbrink@sandia.gov (C.J. Brinker), EMilligan@salud.unm.edu (E.D. Milligan).

molecules [11]. The properties of MSNs include a large surface area (>900 m²/g), large pore volumes (>0.9 cm³/g), a tunable pore size (~1–30 nm), and good chemical and thermal stability; all of which contribute to their suitability for controlled drug release applications. Additionally important, efficient cellular uptake of mesoporous silica particles is size-dependent, with optimal uptake occurring at the sub-micron scale with potential for controlled DNA release [5].

Non-viral spinal gene therapy to suppress neuropathic pain is a relatively new approach that has resulted in successful therapeutic outcomes in a variety of animal models of pathological pain produced by peripheral nerve inflammation and/or trauma from systemic cancer chemotherapeutic administration, peri-sciatic immune activators, or chronic constriction injury [12–16]. However, high transgene doses and limited cargo loading efficiency of polymer platforms were observed, which may minimize the clinical utility of this delivery method. One approach to circumvent these limitations is to deliver therapeutic genes utilizing MSNs for transgene delivery due to their flexibility in cargo loading and release.

In the present work, *in vitro* and *in vivo* long-duration biocompatibility, biodistribution, and functional gene expression following delivery to the spinal cord was conducted using cationic amine-chemically-modified (functionalized) mesoporous silica cores with ~2 nm diameter pores prepared by aerosol-assisted self-assembly, with phospholipid bilayers fused to the core surface. The term 'protocell' will be used to reference MSN-supported lipid bilayers to maintain consistency of nomenclature with the initial published description of their manufacture and characterization [9,17,18]. The principle attractiveness of utilizing these protocells as drug and gene delivery platforms is in their potential for increased drug containment properties, and the tenability of surface chemistry modifications tailored to specific cargos.

2. Materials and methods

2.1. Animals

A total of 62 adult, male Sprague–Dawley rats (Harlan Labs, Houston, TX); 300 ± 5 g were double housed at 21 ± 4 °C in light controlled rooms (12:12 light:dark) and fed standard rodent chow and water available *ad libitum*. All procedures were approved by the Institutional Animal Care and Use Committee (IACUC) of the University of New Mexico, and conducted in accordance to the guidelines recommended by the International Association for the Study of Pain for the handling and use of laboratory animals.

2.2. Behavioral assessment for sensory changes

Baseline spinal cord activity is evaluated using the well-characterized protocol for assessing threshold responses to light touch applied to the hindpaws with a series of calibrated monofilaments (0.4–15 g). The monofilaments generate a touch stimulus when applied to the hindpaw that induces a paw withdrawal response within 8 s [19,20]. Paw withdrawal sensory thresholds are highly sensitive to subtle inflammatory perturbations in the spinal cord, as normal hindpaw response thresholds (5–10 g) are present during healthy, non-pathological conditions [20,21] while response thresholds dramatically decrease (<1 g) in the presence of inflammatory signaling [20,21]. This behavioral response phenotype is used as an indicator of spinal cord health. Prior to behavioral thresholds, rats were habituated to the testing conditions for 4 consecutive days, 1 h/day, in a quiet dimly lit and temperature controlled room (26.0–27.0 °C), where rats were placed on top of an open grid of bars with 2 mm thickness, spaced 8 mm apart to allow access to the entire plantar surface of the hindpaw for tactile stimulation. Response thresholds were determined by a logarithmic series of calibrated Semmes-Weinstein monofilaments (von Frey hairs; Stoeling, Wood

Dale, IL). Testing of behavioral thresholds were conducted identically to that described previously [20,21]. Briefly, baseline (BL) responses to light mechanical touch stimuli were assessed using 10 monofilaments, each with a log-stiffness value, defined as log₁₀ (milligrams × 10), values in grams follow in parentheses: 3.61 (.407), 3.84 (.692), 4.08 (1.202), 4.17 (1.48), 4.31 (2.04), 4.56 (3.63), 4.74 (5.49), 4.93 (8.51), 5.07 (11.75) and 5.18 (15.14). BL values derived from three threshold assessments, at 20 min intervals, were averaged for the right and left hindpaws separately. After injection of protocells, threshold responses were re-assessed at .5, 1, 2, 3, 24 and 72 h. In those rats that underwent unilateral sciatic nerve injury, thresholds were reassessed at 3 and 10 days post-surgery and every 2 days, up to 32 days post-peri-spinal (intrathecal; i.t.) protocell injection. To assess normal food consumption as an indication of general health, body weights were measured following 2, 4, 8, 12, 14, 21, 28, and 56 days following i.t. administration of protocells.

2.3. Chronic constriction injury (CCI)

The surgical procedure for chronic constriction injury (CCI) was performed identically as previously described [22]. Briefly, under isoflurane anesthesia (1.5–2.0 vol.% in oxygen), the mid to lower back and dorsal thigh were shaved and cleaned with diluted Bacti-Stat AE (EcoLab HealthCare Division, Mississauga, Ontario, Canada). Using aseptic procedures, the sciatic nerve was carefully isolated and four chromic gut sutures (Ethicon, Somerville, NJ) were loosely tied around one sciatic nerve. The overlying muscle was sutured closed with two, sterile, silk sutures (Ethicon, Somerville, NJ), and the overlying skin was closed with wound clips. The sciatic nerve of sham-operated rats were identically exposed but not ligated. Animal body weight was recorded and recovery from anesthesia was observed within 10 min.

2.4. Intrathecal (i.t.) injections

Injections were acutely administered and conducted as described previously [14,23]. Briefly, rats were anesthetized with isoflurane (5.0 vol.% in oxygen) and an 18-gauge cannula constructed from an 18-gauge sterile hypodermic needle (Becton Dickinson & Co., Franklin Lakes, NJ) removed from its hub was inserted percutaneously between lumbar vertebrae 5 and 6 (L5–6). During this time, a small amount of cerebral spinal fluid (CSF) efflux from the 18-gauge cannula and a tail flick were observed, indicating subarachnoid catheter placement. A 1 ml Hamilton syringe connected to a 30-gauge, 0.5 inch needle inserted into a catheter composed of a 30 cm-length polyethylene tubing (PE-10; cat# 427401; Becton Dickinson, Sparks, MD) was then used to draw up DOTAP:Chol or DOPC protocells (1.0, 0.1 or 0.01 mg) in a total volume of 20 μl sterile, isotonic saline. The drug-filled PE-10 catheter was then inserted into the open end of the 18-gauge guide cannula and advanced 7.7 mm rostrally, placing the internal portion of the PE-10 catheter at the lumbosacral enlargement of the spinal cord where axon terminals of sciatic afferent nerve fibers synapse onto pain-relevant spinal cord neurons. Injections were given over a 0.5–1 minute interval. Following drug injection, the PE-10 catheter was removed followed by removal of the 18-gauge cannula, and both were discarded. The total time required for these i.t. injections was 2–3 min. All animals displayed full motor activity following recovery from anesthesia.

2.5. Preparation of plasmid DNA

The plasmid vector used in these studies was identical to that previously described [23]. This plasmid's transcriptional cassette consists of a cytomegalovirus (CMV) enhancer/chicken beta-actin (CB) promoter driving the expression of rat IL-10 gene containing a point mutation (F129S) and the SV40 polyadenylation signal. The identical plasmid lacking the IL-10 gene was used as a control (control DNA). Both plasmids were amplified in SURE II competent *Escherichia coli*

(Stratagene, Cedar Creek, TX) and isolated using an endotoxin free Giga plasmid purification kit (Qiagen, Valencia, CA).

2.6. Preparation of mesoporous cationic silica “core” protocells

The mesoporous silica particles were prepared by the surfactant self-assembly method described previously [18,24]. Briefly, a homogeneous solution of the soluble silica precursor, tetraethylorthosilicate (TEOS; Sigma-Aldrich Corp., St. Louis, MO), and hydrochloric acid was mixed in ethanol and water. A surfactant, cetyltrimethylammonium bromide (CTAB; Sigma-Aldrich Corp., St. Louis, MO), with an initial concentration much less than the critical micelle concentration was added to lower the surface tension of the liquid mixture and act as the mesoporous structure-directing template. Aerosol solutions of soluble silica plus surfactant were then generated with nitrogen as a carrier atomizing gas using a commercially available atomizer (Model 9392A, TSI, Inc., St. Paul, MN). The aerosol droplets were solidified in a tube furnace at 400 °C until dry. Once dried, a durapore membrane filter, kept at 80 °C, was used to collect the particles. As a final step, the surfactant was removed at 400 °C for 5 h *via* calcination. The surface of the mesoporous silica core in these studies was chemically modified with 10 wt.% or 15 wt.% by aminopropyltriethoxysilane (APTES; Sigma-Aldrich Corp., St. Louis, MO) conducted identically as previously described [17] to create a positive surface charge to increase loading efficiency of negatively charged cargo. Further, Liu and colleagues report the colloidal stability of these protocells with lipid bilayers, excess amount of liposomes (50 µg liposomes per 0.5 mg silica were used [18]).

2.7. Preparation of liposome-supported bilayers (protocells)

The lipids used in this study were either positively charged, 1, 2-Dioleoyl-3-Trimethylammonium-Propane (DOTAP; cat. # 890890C; Avanti Polar Lipids Inc., Alabaster, AL) or zwitterionic and neutrally charged, 1, 2-dioleoyl-sn-glycero-3-phosphocholine (DOPC; cat. # 850375; Avanti Polar Lipids Inc., Alabaster, AL). Cholesterol (Sigma-Aldrich) was added to DOTAP in a 1:1 ratio (25 mg each), as it has been reported to improve transfection efficiency when included in cationic liposomes [25]. DOTAP:Chol was dissolved in chloroform, followed by evaporation under nitrogen flow. Phospholipids were dissolved in chloroform at concentrations of 10–25 mg/ml. Lipid aliquots of 2.5 mg were placed in scintillation vials. In some experiments where lipids were examined under confocal microscopy, Alexa Fluor 647, a red fluorescent dye (absorption 650 nm and emission 658 nm; Invitrogen, Carlsbad, CA), was added at 2% for these labeling and biodistribution studies. Chloroform was then evaporated under nitrogen flow. The vials were then stored overnight in a vacuum oven to remove remaining chloroform. Samples were stored at –20 °C until used.

To prepare liposomes, vials were brought to room temperature and samples were rehydrated with 1 ml buffer (10 mM MOPS, pH 7.0, 60 mM NaCl) and shaken for 1 h, which resulted in a cloudy suspension. The suspension was extruded through a 100 nm pore diameter membrane with in a mini-extruder (Avanti Polar Lipids), and repeated for a minimum of 21 times. The resulting liquid was placed in a fresh vial and stored at 4 °C until used in the preparation of DNA loaded protocells.

2.8. Preparation of DNA (either 18-bp or pDNA) loaded “protocells”

An 18 bp-DNA oligomer (5'-CTTGAGAAAGGGCTGCCA-3') tagged with 6-carboxylfluorococin (FAM, emission 520 nm, or fluorescein isothiocyanate, FITC emission 488 nm; Invitrogen, Carlsbad, CA) was used to identify the safety profile and anatomical location of protocell cargo following *in vivo* injection. To load the silica core with pDNA *in vivo* behavioral experiments, 35 µl of 200 µM DNA was added to 3.5 mg of cationic silica nanoparticles, gently mixed in sterile 0.5× PBS (25 mg/ml; 140 µl

per 3.5 mg particles) and allowed to incubate for 5 min. In a sterile microcentrifuge tube, 300 µl of 2.5 mg/ml of liposome mixture was added and mixed with the nanoparticle/DNA mixture by pipetting until homogeneous. The resulting mixture was allowed to sit at room temperature for 1 h with occasional agitation by pipetting and then centrifuged for 2 min. at 6000 RPM to remove excess lipids. The supernatant was discarded, and the pellet was washed in sterile PBS followed by centrifugation at 6000 RPM. Pellets (protocell/18mer-DNA-FAM/lipid mixture) were washed 3× and resuspended in sterile PBS at 50, 5 or 0.5 mg/ml. For pDNA loading onto protocells in cell culture experiments, identical steps were followed with DOTAP:Chol lipids resuspended with PBS (pH 7.4) containing 5 µg rat pDNA-IL-10. Following resuspension with PBS (pH 7.4), liposome size and zeta potential were characterized by dynamic light scattering using a Zetatract Ultra151 dynamic light scattering (DLS) instrument (Microtrac Inc., Montgomeryville, PA) and Microtrac FLEX 10.6.1 analysis software. Measurements were made in triplicate using a standard filter with high resolution, high sensitivity and a scan time of 240 s. For *in vivo* behavioral assessment of protocell-delivered IL-10 gene therapy, identical steps described above were followed with DOTAP:Chol lipids resuspended in 50 mg/ml to yield a final dose and concentration of 10 µg pDNA/mg protocell/20 µl PBS.

2.9. Characterization of mesoporous silica particles

Transmission electron microscopy (TEM) images were acquired with a JEOL 2010 200 kV high-resolution transmission electron microscope. The pore diameter was calculated by the Barret–Joyner–Halenda (BJH) method [26]. Particle size distribution of 15 mol% APTES modified mesoporous silica cores as measured by dynamic light scattering. The nitrogen sorption isotherm of the silica particles exhibit a Type IV nitrogen adsorption–desorption isotherms, as previously characterized [27]. Using the Barret–Joyner–Halenda (BJH) model, the pore diameter was determined revealing a narrow distribution. The total surface area was calculated by the Brunauer, Emmett & Teller (BET) method [28].

2.10. Characterization of cargo release-rate from protocells

Mesoporous silica nanoparticles (25 mg) modified with 15% APTES and supporting either a surface coating of DOTAP:Chol 1:1 (DOTAP:Chol) or DOPC lipid bilayer, were dispersed in 1 ml PBS to give a concentration of 25 mg/ml. 12.5 µl of 20 mM dextran-tetramethylrhodamine (DexRho; 10,000 MW, Anionic, Molecular Probes, Invitrogen, Carlsbad, CA, cat# D-1868) to yield ~250 µM. The solution was agitated at room temperature for 45 min, and 50 µl aliquots of each protocell formulation for each timepoint were centrifuged for 2 min, washed 3× with 200 µl of 0.25× PBS to remove unincorporated dye and excess lipids. A total of 200 µl of pH appropriate buffer was added to each sample (N = 3) to give a final concentration of 6.25 µg/µl. The particles and buffers were kept at 37 °C. At designated timepoints, 1, 3, 6, 24, 48, 72, 96 and 168 h (1 week), samples were removed, centrifuged at 14,000 RPM for 2 min to precipitate the silica. A 100 µl sample of supernatant was then transferred into a borosilicate microcuvette to measure absorbance at 555 nm on a Beckman DU 530 UV/vis spectrophotometer (Beckman-Coulter, Inc., Fullerton, CA). In order to determine the quantity of dye released, absorbance readings from the supernatant samples were compared against a set of standards from a serial dilution curve based on known concentrations of dextran-tetramethylrhodamine. The following buffers were brought to a 1 l volume in dH2O to generate the corresponding pH values: 0.1 M acetic acid (pH 2), 0.1 M citrate with 0.03% H2O2 (pH 4), 10.0 mM PBS (pH 7.4), 10.0 mM PBS with 0.1% BSA (pH 8.0), and 0.1 M Amino-Methyl-Propanediol (pH 10).

2.11. Examination of tissue samples by fluorescence microscopy

For tissue collection, rats were euthanized by overdosing with sodium pentobarbital (Abbott Laboratories, North Chicago, IL) at 72 h, and 2, 4 and 8 weeks ($N = 3$ rats for each timepoint and each protocol formulation; DOTAP:Chol or DOPC). Blood samples were taken and mixed with 0.1 ml heparin (APP Pharmaceuticals, LLC, Schaumburg, IL) to prevent clotting. Transcardial PBS (warmed to $\sim 45^\circ\text{C}$; 3–5 min) perfusion was followed by room temperature .01 M PBS; (3–5 min), and then ice cold 4% paraformaldehyde (pH 7.24; 6–8 min) perfusion. Spinal cord, brain, cervical nodes, thymus, spleen, kidney and liver were harvested and post-fixed in 4% paraformaldehyde overnight and transferred to PBS and stored at 4°C . Bone encased spinal cords were placed in 10% ethylenediaminetetraacetic acid (EDTA) solution (~ 3 –4 weeks) to chelate calcium and soften bone for sectioning spinal cord encased in the spinal column to maintain anatomical integrity of the perispinal meninges. The entire spinal cord was cut and cross-sectioned into five, 5 mm, segments starting at the i.t. injection site (pt 0) and proceeding both rostrally and caudally. Brain and organ tissues were cryoprotected in 30% sucrose in (0.1 M PBS + 50 μl 10% sodium azide) for 24 h, embedded in O.C.T. compound in cryomolds (cat# 4565-Sakura Finetek, Torrance, CA), flash frozen in 45°C isopentane on dry ice and finally stored at -80°C until the time of sectioning. For cryosectioning, 10 μm tissue slices were cut on a cryotome, Microm HM 505E (Zeiss, Thornwood, NY), and placed on Vectabond (Vector Laboratories, Burlingame, CA) coated slides.

2.12. Quantitative spectral imaging

For FAM-tagged DNA, multi-spectral tissue imaging and quantification were conducted as previously described [29]. Briefly, images were obtained using an Axioscope microscope connected to a Nuance Camera 2.8 (FX) Multispectral Imaging System (Cambridge Research and Instrumentation Inc., (CRI) Woburn, MA) [29]. This camera contains a liquid crystal tunable filter (LCTF) capable of filtering light from 400 to 720 nm, and can capture a series of images of a particular tissue region at 10 nm wavelength increments. Every pixel of every image (series collected at specific 10 nm wavelength increment) was then analyzed by CRI software to determine its peak spectral intensities from 400 to 720 nm. For each tissue type examined, the software subtracts background autofluorescence, defined as any spectral emission falling outside the 10 nm wavelength range used for analysis. True FAM signal (excitation 494 nm, emission 522 nm) was determined from a control cover-slipped slide on which a small drop of 100 \times diluted FAM-tagged DNA 18-oligomer was placed. The autofluorescence was determined by imaging naive tissue. The intensity of FAM fluorescence across the full wavelength range (400–720) was calculated using the Nuance computer software. A minimum threshold intensity was set automatically by the software and FAM spectral emissions below this point were not included in the calculation. The FAM intensity signal “counts” were then averaged per exposure time (sec) per mm^2 area for each image collected (signal counts/s/ mm^2). An image was acquired for each of 4 slices ($n = 4$) per tissue region (e.g. spinal cord) per rat, and then averaged to generate a mean value for a tissue region per rat ($N = 3$ rats/treatment group). An overall mean value is calculated for each treatment group, and the data are reported as signal counts/s/ mm^2 . Detailed information regarding the computer software can be found on the Caliper Life Science website, a subsidiary of Perkin-Elmer (URL: <http://www.caliperls.com/products/microscopy-imaging-analysis/microscopy-imaging/nuance-fx.htm>).

2.13. Immunohistochemistry

Tissues were collected and sliced identically as described above ($n = 3$ rats with 12 slices per anatomical area). Tissues were permeabilized with 0.5% Triton-X and blocked against non-specific antibody

binding in PBS + 5% BSA + 0.5% Triton-X for 1 h at RT. Primary antibodies were diluted in a solution of PBS with 0.1% BSA, 0.3% Triton-X with 0.1% sodium azide and incubated overnight at RT in a humidity chamber with slight rotation. Primary antibodies were diluted as follows: ED1/CD68 (1:300; a marker for macrophage activity, ED1-cat# SC-7084, Santa Cruz Biotechnology, Santa Cruz, CA); GFAP (1:300, astroglia; cat# AB5804, Millipore, Temecula, CA), Cd11b (microglia/macrophage, 1:300, monoclonal OX42, cat# MCA 275EL, AbD Serotec, Raleigh, NC), and Cleaved-Caspase 3 (Asp175) (apoptotic cells, 1:200, cat#9664 Cell Signaling Technology, Beverly, MA). Slices were washed 3 \times with 0.1 M PBS and then incubated for 2 h at room temperature in a dimly lit room at a 1:200 dilution of a Rhodamine Red-labeled secondary antibody (Jackson Immunoresearch Laboratories, West Grove, PA) in the same solution as that used for primary antibodies. Unbound secondary antibody was removed by 3 \times washes (5 min each in 0.1 M PBS). Slices were then covered with the fluoro-protectant, Vectashield, containing the nuclear stain DAPI (4, 6-diamidino-2-phenylindole) (Vector Laboratories, Burlingame, CA), cover slipped, and stored at 4°C . Three slides, with 3 tissue sections on each slide ($n = 9$), were examined for each primary antibody. As a negative control, no primary antibody was added to an additional slide. A positive control for the Caspase-3 antibody was also included in this experiment. Cultures of Raw 264.7 mouse macrophage cells, a cell type similar to that present in CNS meninges, were treated with bacterial lipopolysaccharide (LPS; 1 $\mu\text{g}/\text{ml}$) for 2 h to initiate apoptosis, and then were subjected to the activated Caspase-3 antibody. Red apoptotic cells stained positively and confirmed the integrity of the Caspase-3 antibody (data not shown). Tissues or cells were examined using an Olympus BX-60 fluorescent microscope, Olympus D71 camera and software (Olympus America, Inc., Center Valley, PA).

2.14. Confocal imaging

To determine subcellular location of FAM-tagged 18 bp DNA loaded onto protocells, or FITC-tagged 18 bp DNA loaded onto liposome-tagged Alexa Fluor 647, 40 \times or 20 \times confocal image z-stacks were obtained with a Zeiss Axiovert 100 inverted microscope (Carl Zeiss Laser Optics, Oberkochen, Germany) using LSM510 Image Acquisition software. The microscope excited the fluorophore of interest DAPI, FAM, FITC, Rhodamine, or Alexa Fluor 647 with one of three lasers: argon–405 nm; NeHe1–543 nm; and HeNe2–633 nm respectively.

2.15. Cellular transfection

For human embryonic kidney cell (HEK 293) cultures, cells were purchased from American Type Culture Collection (ATCC; Manassas, VA-cat# CRL-1573), and maintained in Minimum Essential Medium containing Earle's Salts and l-glutamine (Invitrogen, cat# 11095) to which was added 10% heat inactivated fetal calf serum (FCS) (Gibco, cat#10438) and 100 U/ml penicillin and 100 $\mu\text{g}/\text{ml}$ Streptomycin (Gibco, cat# 15400). Cells were allowed to grow to 80% confluence and were then trypsinized with 0.05% Trypsin-EDTA (Gibco-cat# 15400) to loosen cells. The cell suspension was centrifuged in a sterile 50 ml conical tube at 1500 RPM for 5 min at 4°C . After adding 20 ml of fresh media, the cells were counted by standard technique on a hemocytometer and passed to a new sterile T-75 flask, plated at 10.0–15 \times 106 at each pass. Cells were incubated at 37°C with an atmosphere of air, 95% and CO₂, 5% until experimental procedures.

For transfection with protocells, HEK 293 cells were plated at 1.0 \times 10⁶ cells/ml on 24 well sterile poly-D lysine coated culture plates (Becton Dickinson, Twin Oak Park, Bedford, MA) in 1 ml sterile MEM or DMEM respectively, both supplemented with 10% heat inactivated FCS and 100 U/ml penicillin and 100 $\mu\text{g}/\text{ml}$ streptomycin and allowed to grow 24 h to 80% confluence. Media was exchanged with 1 ml fresh media containing 500, 50, 25, 10, and .5 $\mu\text{g}/\text{ml}$ DOTAP or DOPC protocells loaded with pDNA-IL-10-GFP (5, 0.5, 0.25, 0.1 or

0.05 $\mu\text{g}/\text{ml}$), pDNA-IL-10 (5, 0.5, 0.25, 0.1 or 0.05 $\mu\text{g}/\text{ml}$). In a separate experiment, media was exchanged with 1 ml fresh media containing LPS (10 ng), naked pDNA-IL-10 (5 μg), or DOTAP:Chol + pDNA-IL-10 (5 μg) lacking the mesoporous silica core. The protocell containing media was removed after 5 h and replaced with fresh media. Media was collected 24 h later and analyzed for GFP transfection (green fluorescence) and/or IL-10 protein release using rat IL-10 specific Quantikine™ ELISA kit (R&D Systems, Minneapolis, MN) according to manufacturer's instructions, or immunostaining with IL-10 primary antibody (R&D Systems, Minneapolis, MN) with Rhodamine 2° antibody in a procedure identical to that used for the immunohistochemical staining outlined above.

2.16. Cell viability assay

HEK 293 cells were plated at $5\text{--}6 \times 10^6$ cells/ml on 24-well sterile poly-D lysine coated culture plates (Becton Dickinson, Twin Oak Park, Bedford, MA) in 1 ml sterile MEM supplemented with 10% heat inactivated FCS, 100 U/ml penicillin and 100 $\mu\text{g}/\text{ml}$ streptomycin, and allowed to grow to 80% confluence. Media was removed and 1 ml of fresh media was added containing 500, 50, 25, 10, and .5 $\mu\text{g}/\text{ml}$ DOTAP or DOPC protocells loaded with pDNA-IL-10-GFP, or blank protocells. The media was removed after 5 h and replaced with fresh media and the cells were allowed to incubate for an additional 21 h. Cells were removed with a standard sterile cell scraper and 500 μl of cell suspensions placed in a flow cytometry tube on ice (Falcon cat# 352008—Becton Dickinson Labware, Franklin Lakes, NJ). Saponin (0.1%) was used to induce cell death for assay to compare against other experimental manipulations. 3 min before examination by flow cytometry (FacsCan4, Becton Dickinson), 50 μl of 10 μM ethidium-homodimer D-1 was added to label dead cells.

2.17. Mouse macrophage (Raw 264.7) cells for nitric oxide assay

Raw 264.7 cells were obtained from American Type Culture Collection (ATCC, Manassas VA, USA—cat# TIB-71) and cultured as adherent cells in Dulbecco's Modified Eagle's Medium (Sigma-Aldrich, cat# D6429) supplemented with 10% heat-inactivated fetal bovine serum (Gibco, cat# 10082-147) and 100 U/ml penicillin and 100 $\mu\text{g}/\text{ml}$ streptomycin (Gibco—cat#-15140122) and maintained at 37 °C under humidified 5% CO₂ atmosphere. Cells were grown to 85% confluency, collected by scraping, and sub-cultured for 3 passages. For these experiments, dead cells were counted by hemocytometer using trypan blue exclusion.

2.17.1. Measurement of nitric oxide production

Raw 264.7 cells were seeded at a density of 2.75×10^5 cells/ml in 24 well plates 24 h prior to experimentation and maintained at 37 °C under humidified 5% CO₂ atmosphere. At 85% confluency, the supernatant was exchanged with DMEM containing different formulations of DMEM and protocells or protocell constituents and followed by a 2 h incubation then washed twice in PBS (pH 7.4, Gibco—cat# 10010). Wells treated with 10 ng/ml lipopolysaccharides from *E. coli* (LPS, Sigma-Aldrich, cat# L6529) were exposed to DMEM containing LPS for 10 min followed by removal and washed twice in PBS. Nitric oxide production was measured using the commercially available Griess Reagent System (Promega, USA, cat#-G2930) according to the manufacturer's instructions. Absorbance was measured at 550 nm using a Tecan Infinite® plate reader (Tecan Systems, Inc., San Jose, CA). All experiments were run in triplicate.

2.18. Data analysis

Psychometric behavioral analysis was performed as previously described [20] to compute the absolute threshold that resulted in the 50% hindpaw withdrawal response. As described previously [20,21,30]

withdrawal thresholds were determined by using the software program, PsychoFit. The software for PsychoFit may be downloaded from L.O. Harvey's website (<http://psych.colorado.edu/~lharvey>). This program fits the pattern of hindpaw responses for each timepoint to a Gaussian integral psychometric function and generates a 50% threshold value for that timepoint. As such, parametric statistical analyses (repeated measures ANOVA) are applied to determine the statistical significance between treatment groups at multiple timepoints using the computer software, GraphPad Prism, version 4.03 (GraphPad Software Inc., San Diego, CA). All other statistical analyses were performed using the computer software, GraphPad Prism, version 4.03 (GraphPad Software Inc., San Diego, CA). All data is expressed as mean \pm SEM. Post hoc analysis was completed using Bonferroni's test.

3. Results

Mesoporous silica particle cores were prepared by the surfactant templated aerosol-assisted self-assembly method previously developed and communicated [18]. The resulting hydrophilic nanoparticles were further modified with APTES and characterized by a uniform, ordered and connected mesoporosity (Fig. 1A), with a positive of 24 ± 5 mV in $0.5 \times$ PBS, or when fused with DOTAP:Chol or neutral DOPC, 4.5 mV \pm 2.2 mV or -11.4 ± 3.6 mV, respectively. The average size is ~ 230 nm with a specific surface area of 935 m²/g and pore diameter of 2–5 nm (Fig. 1B, D). Cryogenic TEM image reveals the liposome bilayer that is ~ 4 nm thick (white arrows, Fig. 1C). Protocells formulated with DOPC lipids resulted in a cargo loading of dextran tetramethylrhodamine (DexRho) at a capacity of ~ 13.49 μg and protocells formulated with DOTAP:Chol lipids exhibited a cargo loading capacity of ~ 16.12 μg DexRho.

Protocells with either DOPC or DOTAP:Chol formulations were characterized separately for their release of DexRho cargo, in which separate aliquots were individually incubated in pH solutions ranging from 2 to 10 for durations of 1 to 168 h (Table 1 and Fig. 1F, G). Both DOPC and DOTAP:Chol formulated protocells revealed an increase in cargo release at pH 7.4 compared to 6.0 that continued through 24 and 48 h, respectively (Fig. 1F, G). Both pH 6 and pH 7.4 simulate pH environments present extracellularly or in endosomal compartments. Additionally, a characterization of DOPC and DOTAP:Chol formulated protocells loaded with DexRho cargo at a full range of pH levels (Table 1) is provided to determine cargo stability under disparate conditions that can occur during unique manufacturing conditions or under highly acidic conditions that are present during cellular inflammatory processes.

3.1. In vitro cellular viability is substantial

Cells remain viable following application of protocells formulated with DOTAP:Chol or DOPC. HEK cells were incubated with 10–500 $\mu\text{g}/\text{ml}$ protocells formulated with DOTAP:Chol or DOPC containing plasmid DNA encoding the anti-inflammatory cytokine, interleukin-10, and the reporter gene, green fluorescent protein (pDNA-IL-10/GFP; 10 $\mu\text{g}/\text{mg}$ protocells) for 24 h. Protocells without cargo served as controls. To examine the effects of DOTAP:Chol or DOPC protocells containing pDNA-IL-10/GFP cargo on cellular viability, flow cytometry was used by applying ethidium-homodimer-1 (EH-1) to stain the cells. EH-1 enters the cell nucleus and intercolates with DNA only in dead or dying cells in which the membrane is breaking down. Thus, EH-1 does not interact with DNA of live cells with intact membranes. Excitation of EH-1 at 528 nm leads to 617 nm emission (red fluorescence), which is detected by the flow cytometer, and each dead cell is counted. The percentage of dead cells is quantified per 10,000 cells. The percent of live cells was determined (Fig. 2). Cells left untreated served as an index of basal cell viability, which was observed to be $> 98\%$. To ensure dead cell quantification, a separate group of cells were treated with 0.1% saponin,

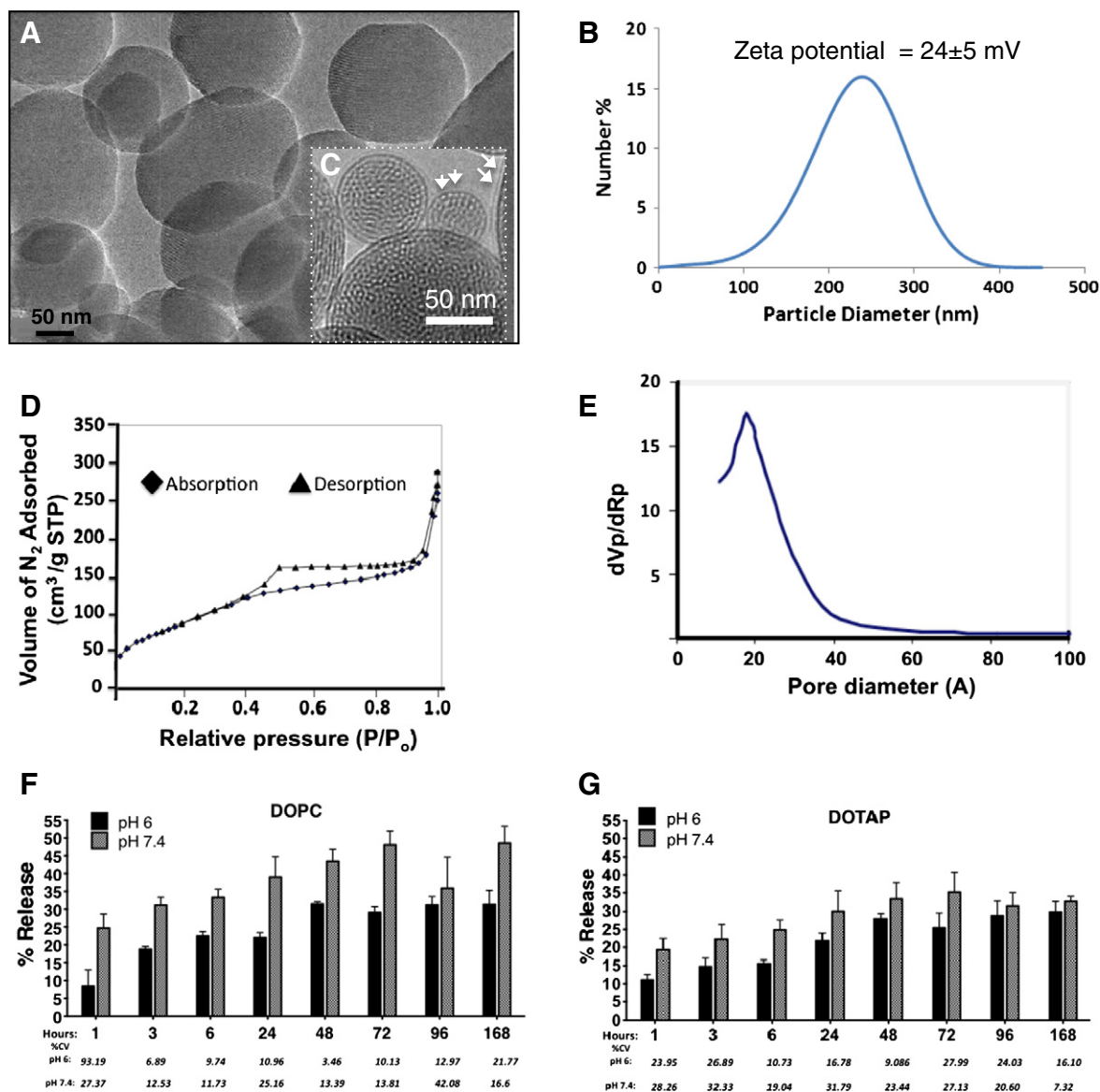


Fig. 1. Characterizations of protocells. (A) TEM image of mesoporous silica nanoparticles; scale bar = 50 nm. (C) Inset: Cryogenic TEM image revealing the liposome bilayer that is ~4 nm thick (white arrows); scale bar = 50 nm. (B) Particle size distribution of 15 mol% APTES modified mesoporous silica cores as measured by dynamic light scattering. The average particle diameter of the mesoporous silica cores is 230-nm with a rather wide particle size distribution reflecting that of the aerosol generator. The surface of the mesoporous silica core in these studies was chemically modified with 15 mol% aminopropyltriethoxysilane (APTES) to impart a positive surface charge (24 ± 5 mV in $0.5 \times$ PBS) that increases loading efficiency of negatively charged cargo. When fused with positively charged DOTAP/DOPC or neutrally charged DOPC-based liposomes, the surface charge was measured in $0.5 \times$ PBS to be 4.5 mV \pm 2.2 mV or -11.4 ± 3.6 mV, respectively. (D) Nitrogen sorption isotherm of 15% aminated silica nanoparticles is a type IV isotherm with a narrow hysteresis loop, typical of a 2D hexagonal mesoporous silica. (E) The pore diameter was determined to be 2–5 nm with a narrow distribution using the Barrett–Joyner–Halenda (BJH) model. The Brunauer–Emmett–Teller (BET) surface area is ~ 935 m²/g, with a pore volume ~ 0.48 cm³/g and the porosity of 0.52. (F) DOPC protocells and (G) DOTAP:Chol protocells examined from 1 to 168 h at pH 6 and 7.4 ($N = 3$ samples/pH values/timepoint). The negatively charged fluorophore, dextran tetramethylrhodamine (DexRho) loaded protocells served as anionic cargo. For DOPC protocells, cargo release time-dependently increased to 24 h and remained relatively stable (~ 45) thereafter through 168 h ($F_{(7,32)} = 8.728$; $p < 0.0001$), with initially greater cargo release at pH 7.4 than at pH 6.0 ($F_{(1,32)} = 51.0$; $p < 0.0001$). DOTAP:Chol protocell cargo revealed a similar release pattern to DOPC protocells with the exception that increased cargo from DOTAP:Chol continued to increase through 48 h ($F_{(7,32)} = 6.98$; $p < 0.0001$) with release appearing consistent thereafter. Also similar to DOPC, cargo release from DOTAP:Chol protocells is initially greater at pH 7.4 compared to pH 6.0 ($F_{(1,32)} = 15.42$; $p < 0.001$). Thus these data suggest that cargo retention is greatest at pH 6.0 in both DOPC and DOTAP:Chol formulated protocells. Note: while standard error of the mean (SEM) is provided indicating sample variance, % confidence interval (%CV) is additionally provided along the X-axis. The pattern of greater cargo release that is somewhat pH sensitive for the first several days suggests that time and pH may be important factors that influence initial drug-delivery kinetics.

and only ~3% remained viable. Protocells formulated with either DOTAP:Chol or DOPC resulted in <5% dose-related decrease in cell viability compared to live controls and remained stable even at the highest dose of 500 μ g/ml. Thus, cells exposed to DOTAP:Chol or DOPC protocells remained healthy, suggesting that DOTAP:Chol or DOPC protocells lack overt toxicity *in vivo*.

3.2. Spinal delivery of protocells is well tolerated in an animal model

Light touch sensory threshold assessment is highly sensitive to subtle perturbations in spinal cord homeostasis. Increases in local spinal immune signaling molecules lead to spinal sensitization of pain-related projection neurons resulting in a hypersensitivity to light

Table 1

Characterization of anionic DexRho-loaded DOPC and DOTAP:Chol protocells at various pH values over time. To fully characterize the stability of cargo release at extreme pH values as well as at physiologically relevant pH values, DexRho cargo release was examined at discrete timepoints at pH values ranging from 2 to 10. The samples (N = 3/conditions) were averaged (mean) and the sample variance is presented (SEM) as well as the sample % coefficient of variation (%CV) that provides comparisons between independent datasets that are sensitive to small changes in the sample means. Compared to DOTAP:Chol formulated protocells, the cargo from DOPC formulated protocells at pH 2 is retained across time, while similar to DOTAP:Chol, the greatest cargo release is observed at pH 10 that moderately increases with time. Thus, both protocell formulation (DOTAP:Chol and DOPC) and pH significantly influence cargo release over time ($F_{(77,192)} = 1.60$; $p < 0.01$).

Lipid formulation	pH 2				pH 4				pH 8				pH 10			
	DOTAP:Chol		DOPC		DOTAP:Chol		DOPC		DOTAP:Chol		DOPC		DOTAP:Chol		DOPC	
Hours	Ave	SEM/%CV	Ave	SEM/%CV	Ave	SEM/%CV	Ave	SEM/%CV	Ave	SEM/%CV	Ave	SEM/%CV	Ave	SEM/%CV	Ave	SEM/%CV
1	30.22	5.01/23.36	18.90	7.57/56.45	30.12	1.61/7.55	24.54	6.62/38.03	38.41	6.24/22.92	37.97	0.68/2.53	37.20	7.72/29.27	50.53	5.64/15.73
3	31.09	2.18/9.87	24.36	2.34/13.54	34.45	1.31/5.38	23.33	8.48/51.30	47.26	5.68/16.96	38.38	4.53/16.65	47.86	6.53/19.24	56.54	7.39/18.82
6	23.47	0.64/3.86	22.23	2.01/12.72	31.94	6.39/28.19	34.43	7.18/29.40	42.68	6.94/22.93	48.02	4.38/12.88	48.68	9.24/26.76	66.68	5.82/12.3
24	23.15	0.05/0.32	18.99	1.23/9.12	38.75	3.83/13.94	35.41	7.69/30.60	39.68	7.68/27.28	51.97	4.63/12.57	67.07	8.10/17.03	79.69	10.95/9.38
48	26.35	3.24/17.35	17.09	2.45/20.23	45.58	2.26/7.0	39.07	6.86/24.75	43.60	7.30/23.62	54.93	9.17/23.54	71.40	12.58/24.84	77.16	7.26/13.26
72	28.42	1.32/6.53	17.92	3.23/25.39	45.82	2.22/6.84	29.09	8.11/39.29	47.39	8.68/25.83	42.88	2.94/9.68	81.17	11.44/19.87	77.69	11.36/20.61
96	31.07	4.53/20.56	17.04	2.04/16.87	40.88	1.07/3.68	39.47	8.58/30.64	52.06	8.69/53.53	51.81	11.92/32.44	78.29	13.38/24.11	73.45	1.49/2.85
168	38.60	2.30/8.38	12.05	4.75/55.63	42.05	3.05/10.23	28.49	7.69/38.06	50.45	6.49/18.13	50.50	10.29/28.73	81.48	11.36/19.66	91.17	9.49/14.67

touch stimuli applied to the body area innervated by axons whose central terminals also project to the affected spinal segment [19,20]. Thus, assessing alterations in light touch thresholds from basal values following central nervous system protocell application can be a timely, robust and reliable *in vivo* examination of protocell early-phase toxicity within the local spinal cord compartment. Baseline (BL) sensory threshold values for both hindpaws were recorded prior to an i.t. injection of DOTAP:Chol or DOPC formulated protocells. Thresholds close to 10 g of stimulus intensity were observed in all rats prior to treatment (Fig. 3).

Following an i.t. injection of 0.01 or 1 mg DOTAP:Chol formulated protocells, a small increase in light touch sensitivity of the left paw was observed at 30 min and rapidly recovered to basal levels and remained stable during a 72 hr observation period (Fig. 3A, B). Normal insignificant basal variations in paw thresholds were observed in 0.01 mg protocell and control (Vehicle) injected rats. Conversely, both 0.01 and 1 mg DOPC formulated protocells induced a small increase in light touch sensitivity (values dropped to <1.0 g stimulus intensity) in both the left and right hindpaws at 2 h, that mostly recovered to BL values during the remaining 72 h observation period (Fig. 3C, D). The transient 2-hr increase in light touch sensitivity following DOPC formulated protocells was unexpected given reports show that *in vitro*, DOPC toxicity is virtually absent. However, *in vivo* subtle changes in the local spinal milieu may occur to a greater

extent that alters early-phase toxicity and corresponding neuronal processing of normal sensory stimuli. Nevertheless, normal body weight gain was observed in all rats throughout an 8 week observation period during which time, animals remained active and well-groomed (Fig. 3E). Taken together, these data support that i.t. administration of DOTAP:Chol, lack alterations from normal sensory processing and both DOTAP:Chol and DOPC formulated protocells are well-tolerated in the peri-spinal region of rats.

3.3. Intrathecal (i.t.) DNA delivered by DOTAP:Chol or DOPC protocells remains closely associated with meninges

Non-coding 18 bp oligonucleotide DNA labeled with the fluorophore, FAM (Ex/Em 492/517 nm; green) delivered by either DOTAP:Chol or DOPC formulated protocells remained closely associated with the cells of the meningeal layer in the spinal cord, but did not penetrate tissue parenchyma. A representative spinal tissue section near the i.t. injection site, revealed DOTAP:Chol protocells containing FAM-tagged DNA (green) in/adjacent to the meningeal layer (Fig. 4A–D), with cellular nuclei counter-stained with the nuclear specific fluorophore, DAPI. Glial cell astrocyte processes and endfeet (astrocytes stained for glial fibrillary acidic protein, GFAP; red) are typically present at the neural-pial meningeal interface, which are capable of taking up extracellular material. Yet, no co-localization of FAM-tagged DNA protocell cargo within astrocytes was observed (Fig. 4A, white arrow). However, immune-relevant macrophage and microglia that normally reside in meninges and at the neural-pial interface are highly efficient phagocytic cells. Indeed, FAM-tagged DNA containing protocells robustly co-localized with macrophages/microglia (stained for CD11b antigen expression; red) in the meningeal peri-spinal region. Co-localization appears yellow (Fig. 4B, white arrow). While microglia are present (red) in the deeper spinal parenchyma, FAM-tagged DNA is absent (Fig. 4B).

Caspase-3 is a well-characterized enzyme that plays a critical role in the late stages of programmed cell death (apoptosis). Immunohistochemical detection of Caspase-3 (red) was entirely absent in the spinal cords and brains of rats where DOTAP:Chol formulated protocells were present. A representative image of protocells containing FAM-tagged DNA (green) in the meninges reveals no positive Caspase-3 immunoreactivity at 8 weeks following i.t. injection (Fig. 4C). Confocal examination of meningeal macrophage/microglial cells immunostained for expression of ED1, a marker for active immune cells, revealed that DOTAP:Chol protocells containing FAM-tagged DNA were closely associated with the DAPI-stained peri-nuclear area of ED1 expressing cells (Fig. 4D, white arrow).

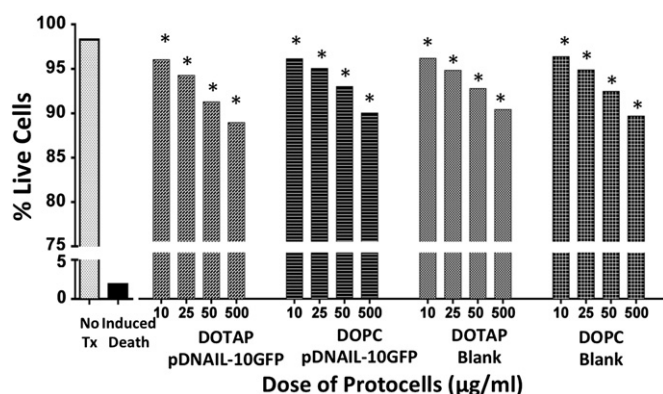


Fig. 2. Cells remain highly viable following application of DOTAP:Chol and DOPC protocells containing pDNA-IL-10-GFP. Cells were incubated for 24 h with DOTAP:Chol or DOPC protocells loaded with pDNA-IL-10-GFP or blank control protocells (no pDNA) at varying concentrations across a 50-fold dose range, 500, 50, 25 and 10 µg/ml. Dead cells were identified by flow cytometry after staining with ethidium-homodimer-1. Results are representative of the percentage of gated cells (average of 4 experiments) compared to untreated control cells, ** $p < 0.01$; and *** $p < 0.0001$.

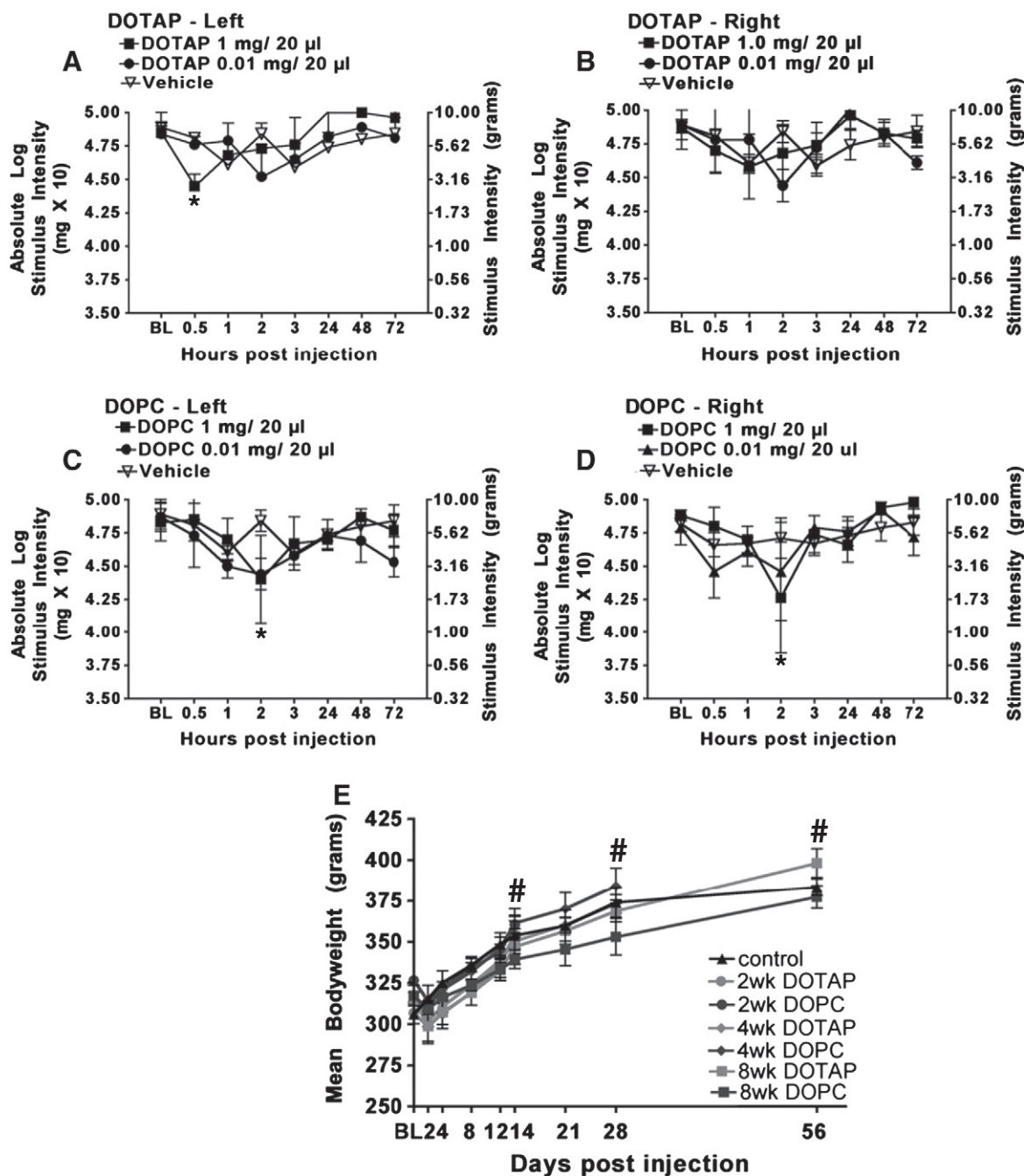


Fig. 3. *In vivo* characterization of the biocompatibility between DOTAP:Chol and DOPC protocells. For clarity, protocell type (DOTAP vs. DOPC) is separated and represented in graphs identified as DOTAP or DOPC data, while the identical vehicle-treated group (assessed alongside the protocell-treatment groups during experimentation) is represented with both the DOTAP- and DOPC-treated animals. (A–D) Baseline (BL) threshold responses of both hindpaws (left and right) between all animal groups were similar ($F_{(9,20)} = 0.288$; $p = 0.97$). (A, B) Following i.t. injection with either 1 or 0.01 mg of DOTAP:Chol or vehicle, left hindpaw threshold responses remained unchanged throughout the timecourse (0.5, 1, 2, 3, 24, 48 and 72 h) ($F_{(6,24)} = 1.63$; $p = 0.181$), however, right hindpaw thresholds were moderately reduced ($F_{(6,24)} = 3.45$; $p < 0.05$). Post-hoc analysis revealed that thresholds responses 30 min after DOTAP protocell injection were significantly lower than vehicle treated animals ($p < 0.05$). (C, D) For DOPC-treated animals, while an overall decrease in thresholds was not observed across the timecourse in left ($F_{(24,60)} = 1.88$; $p > 0.05$) or right hindpaws ($F_{(24,60)} = 1.01$; $p > 0.05$), a small and significant decrease at 2 h in both hindpaws was observed ($p < 0.05$). Throughout the 8-week observation, all animals exhibited normal grooming, activity, exploratory behavior and body weight gain following i.t. injection with DOTAP:Chol or DOPC protocells. (E) At BL, there was no significant difference in body weight between untreated (black triangles) and treated animals that received i.t. DOTAP:Chol (2 weeks, solid gray circles; 4 weeks, solid gray diamonds; 8 weeks, solid gray squares) or DOPC protocells (2 weeks, solid black circles; 4 weeks, solid black diamonds; and 8 weeks, solid black squares) ($F_{(6,14)} = 2.837$, $p > 0.05$). Consistent and normal gain in body weight compared to their BL levels was observed prior to sacrifice at 2 weeks ($F_{(10,30)} = 3.02$, $p < 0.0001$), at 4 week ($F_{(14,42)} = 2.62$, $p < 0.0001$), and at 8 weeks ($F_{(16,48)} = 3.65$, $p < 0.0001$) during an 8-wk observation period occurred in control animals and those receiving protocells by i.t. injection ($n = 3$ per group). * $p < 0.05$; and # $p < 0.0001$.

To ascertain whether the 18-bp DNA cargo remains associated *in vivo* with mesoporous silica liposome-supported bilayers, DOTAP:Chol liposomes were labeled with Alexa fluor-647 and adsorbed to silica cores loaded with FITC-labeled 18-bp DNA. Rats were given a single spinal i.t. injection of protocells (1 mg) and sacrificed 72 h

later to identify protocell lipid bilayers colocalized to the DNA cargo under confocal microscopy. DNA cargo (green) is robustly observed in the meninges surrounding the i.t. injection site (Fig. 4E), and DOTAP:Chol supported liposomes (red) are identified in the perispinal meninges (Fig. 4F). Light microscopy reveals the spinal tissue

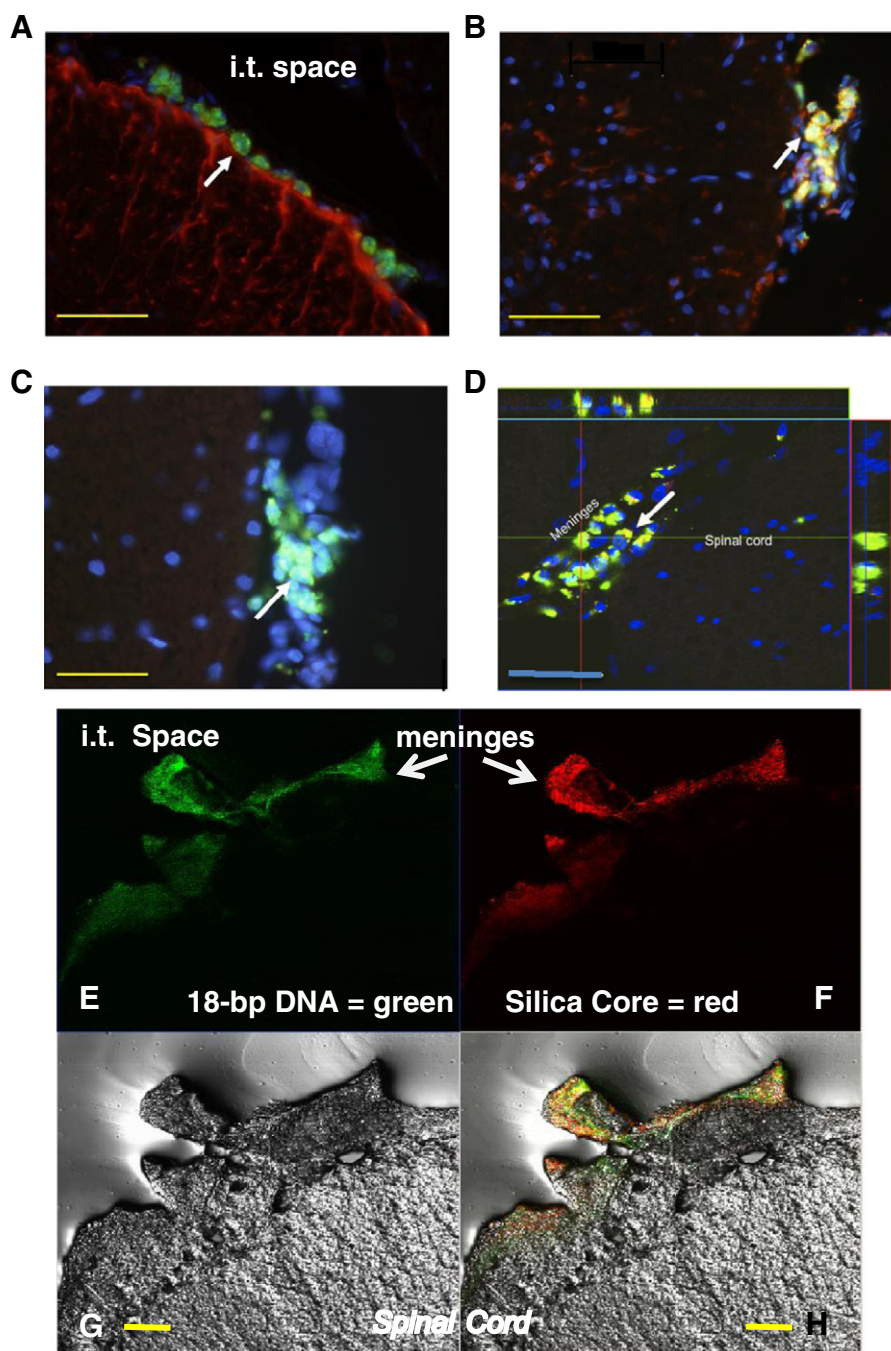


Fig. 4. Histological examination of DOTAP:Chol protocells with 18-bp FAM-labeled DNA cargo in the spinal cord. Fluorescent histological examination of spinal cord sections near the lumbar spinal cord injection site (segments L3–4) 8 weeks after i.t. injection of DOTAP:Chol protocells loaded with DNA cargo (2 μ g). (A) Protocells containing DNA cargo (green; white arrow) are not colocalized with astroglia stained for glial fibrillary acidic protein, GFAP (red) and do not penetrate the spinal parenchyma, but are localized to the spinal pia and arachnoid matter. (B) Protocells localized to the peri-spinal meninges containing cells stained with the microglia/macrophage antigen expression protein, Cd11b (red). Colocalization of Cd11b with DNA cargo (green) is observed as yellow (white arrow). (C) There is no evidence of cellular death in tissue in contact with protocells, as indicated by the absence of positive staining for the apoptotic marker, activated Caspase 3 (red) while protocell-containing DNA cargo (green; white arrow) is clearly present in the peri-spinal meninges. (D) Confocal image identifying DOTAP:Chol protocell cargo of FAM-labeled DNA (green) in the peri-nuclear area (cell nuclei stained with DAPI; blue) of meningeal macrophage cells stained for the classic activation marker, EDI (red; white arrow) in the dorsal spinal cord meninges. Overlap reveals yellow cytoplasmic and peri-nuclear staining. All images are at 20 \times ; scale bar = 40 μ m. (E–F) Confocal images identifying single-stranded FITC-labeled DNA cargo (2 μ g) loaded onto DOTAP-formulated protocells with DOTAP labeled with Alexa-fluo 647, which is visualized only under UV light (red). (E) The confocal fluorescent images reveal the presence of protocell cargo (green DNA) and (F) DOTAP:Chol liposome (Alexa-fluo 647, far red) in meninges at the site 3 days following intrathecal injection. (G) The identical tissue region collected with light differential interference contrast (DIC) and (H) an overlay of both fluorescent and DIC to verify co-localization of silica-supported DOTAP:chol and its DNA cargo. Images are 10 \times ; scale bar = 40 μ m.

architecture (Fig. 4G) and an overlay of the confocal fluorescent image reveals clear colocalization of DNA cargo with liposomes (yellow) (Fig. 4H), suggesting that the protocell-cargo formulation is stable for 72 h *in vivo*.

3.4. *In vivo* biodistribution of protocells

Eight weeks following i.t. injection, protocells remain in the CNS and are not found in peripheral tissue. As the animals appeared to

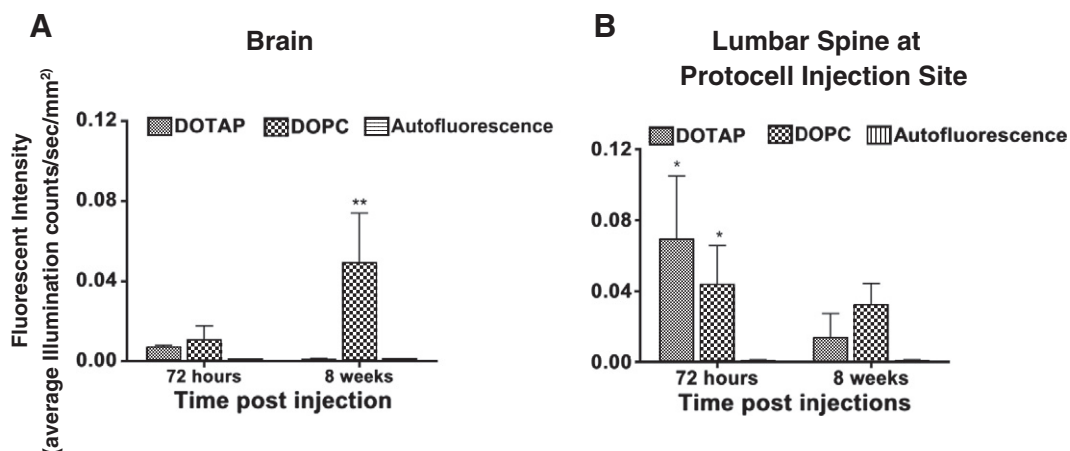


Fig. 5. The lipid bilayer formulation of the protocell determines the degree of spread throughout the CNS following an i.t. injection. Graphs are representative of the key data in the corresponding Table 2. Fluorescent spectral signal from FAM-labeled 18-bp DNA cargo in cryostat-sliced tissue sections (n = 4) of DOTAP:Chol or DOPC protocell i.t. treated animals is compared to the spectra of background autofluorescence from naïve animals. (A) In the brain at 72 h, no significant signal from FAM-tagged DNA delivered by either DOTAP:Chol or DOPC protocells was observed. However, by 8 weeks, compared to DOTAP:Chol protocell treated tissue and autofluorescence, FAM-labeled DNA delivered by DOPC protocells had significantly increased ($F_{(2,6)} = 8.60$; $p = 0.0173$). (B) In the lumbar spinal cord, DNA delivered by both DOPC and DOTAP:Chol protocells was present at both 72 h and 8 weeks (FAM signal analysis vs. autofluorescence, $F_{(2,6)} = 6.18$; $p = 0.0348$), with DNA levels at 72 h significantly higher than those at 8 weeks ($F_{(1,6)} = 10.71$; $p < 0.02$).

experience no adverse effects from DOTAP:Chol or DOPC formulated protocells, even at the highest dose, the biodistribution of protocells within and outside of the central nervous system (CNS) was quantified. In these experiments, rats received an i.t. injection of DOTAP:

Chol or DOPC protocells loaded with FAM (1 µg FAM 18 bp DNA oligomer/1 mg protocells), and tissues were harvested 2, 4, and 8 weeks later. Blood, the immune organs (cervical lymph nodes, thymus and spleen), the filtering organs (kidney and liver), as

Table 2
Values ($1 \times E-04$) of each anatomical region are an average of computer-generated spectral analyses taken from 4 separate images of four 10 µm cryostat sliced tissue sections. Yellow boxes indicate those areas in which the signal from FAM-labeled DNA cargo reached levels that were significantly higher than control autofluorescence for that tissue. Asterisks indicate the amount of significance. At 72 h and 8 weeks, very low levels of DOPC or DOTAP:Chol protocells were detected in the blood (data not shown), thymus, spleen, liver and kidney, while measurable amounts of DOTAP:Chol and DOPC were detected in the CNS.

Biodistribution of fluorescent tagged 18 bp DNA: Qualification by spectral analysis (values $1 \times E-04$)										
	Auto fluorescence		72 hours				DOTAP		DOPC	
	Mean	SEM	Mean	SEM	Mean	SEM	Mean	SEM	Mean	SEM
Inside CNS										
¹ Brain	1.53	0.136	65.3	14.6	104	72.3	7.2	7.2	**491	0.248
Cervical spine	2.62	0.158	15.6	11.4	119	110	2.68	1.5	**580	359
10 mm rostral	22	16.2	624	232	682	262	26.7	5.7	286	16.4
² Lumbar	6.6	5.9	*689	359	*434	222	*134.8	0.013	*320.2	121.9
5 mm caudal	17.7	10.5	325	147	230	175	17.1	9.69	***2419	259.9
1.5 mm caudal	10.5	5.8	194	76.7	158	169	24.5	1.23	***2111	274.1
2.5 mm caudal	7.14	3.45	*203	68.7	*250	55	3.16	0.625	2737	519
Peripheral Tissues										
Nodes	0.11	1.5	19.2	11.7	12.3	1.34	8.01	4.61	4.2	2.6
Thymus	13.3	6.8	*1044	471	648	97.4	9.4	0.657	16.4	4.66
Spleen	10.5	0.422	*45.2	10.07	10.4	12.69	12.2	12.7	6.2	1.8
Liver	25.2	3.7	24.1	4.87	36.6	6.45	14.6	0.395	18.7	2.65
Kidney	96.2	2.93	1.13	1.5	10.5	0.244	8.92	0.587	11.7	1.21

*p < 0.05.
**p < 0.01.
***p < 0.0001.

well as sections from the brain, cervical, thoracic and lumbar spinal cord were examined to quantify protocells by spectral microscopy analysis that allows computerized de-convolution and quantification of the true FAM-signal from background autofluorescence (Fig. 5 and Table 2).

The blood was negative for FAM detection (data not shown). The highest amount of FAM levels at 72 h post-DOPTAP:Chol or DOPC protocell injection was observed at the i.t. injection site in the lumbar spinal cord, which significantly decreased by 8 weeks (Fig. 5B). Only DOPC formulated protocells containing FAM-tagged DNA accumulated in the brain by 8 weeks (Fig. 5A). Thus, differences in the biodistribution between the two protocell lipid formulations were observed. Also at 8 weeks, the DOTAP:Chol protocell FAM signal had diminished and was only significant locally, near the injection site, suggesting that DOTAP:Chol formulated protocells may be optimal to maintain localized drug effects, while leaving the brain and the body primarily undisturbed.

Outside the central nervous system, FAM signal was negligible including in the liver and kidney. At 72 h, a minor but significant amount of FAM was detected in the thymus following treatment of both DOTAP:Chol and DOPC formulated protocells. The data represented in Fig. 5A and B are included in Table 1 to provide relative comparisons in FAM detection levels with respect to FAM levels observed in other tissue regions that in most cases, appear negligible. These data additionally suggest that a large amount of protocells

escape the intrathecal compartment and are eliminated within 3 days, as protocells are absent from these tissue systems at this timepoint.

3.5. Protocell IL-10 gene delivery leads to robust transgene expression

Transfection of HEK cells with a bicistronic plasmid containing the gene for IL-10 and GFP successfully resulted in the expression of IL-10 (Fig. 6A) as well as GFP (Fig. 6C, inset), indicating functional IL-10 transgene expression in GFP expressing HEK cells. Protocells formulated with either DOTAP:Chol or DOPC and loaded with plasmid DNA encoding the IL-10 gene alone (pDNA-IL-10) or in combination with the reporter gene, pDNA-IL-10/GFP, were incubated with HEK cells to examine transgene IL-10 protein expression. It is important to note that HEK cells do not produce IL-10 protein thus providing a reliable assay to quantify transgene-specific IL-10 gene activation. Surprisingly, only those protocells formulated with DOTAP:Chol containing pDNA-IL-10 or pDNA-IL-10/GFP resulted in a robust dose-dependent increase in protein IL-10 levels compared to untreated controls, with the greatest amount of protein (~900 pg/ml) produced following incubation with 500 µg/ml DOTAP:Chol formulated protocells. In contrast, IL-10 protein from transgene IL-10 delivered by DOPC protocells containing either pDNA-IL-10 or pDNA-IL-10-GFP was significantly lower and reached maximal values of no greater than 100 pg/ml. Additionally, naked pDNA-IL-10 or DOTAP:Chol + pDNA-IL-10 resulted a dramatically

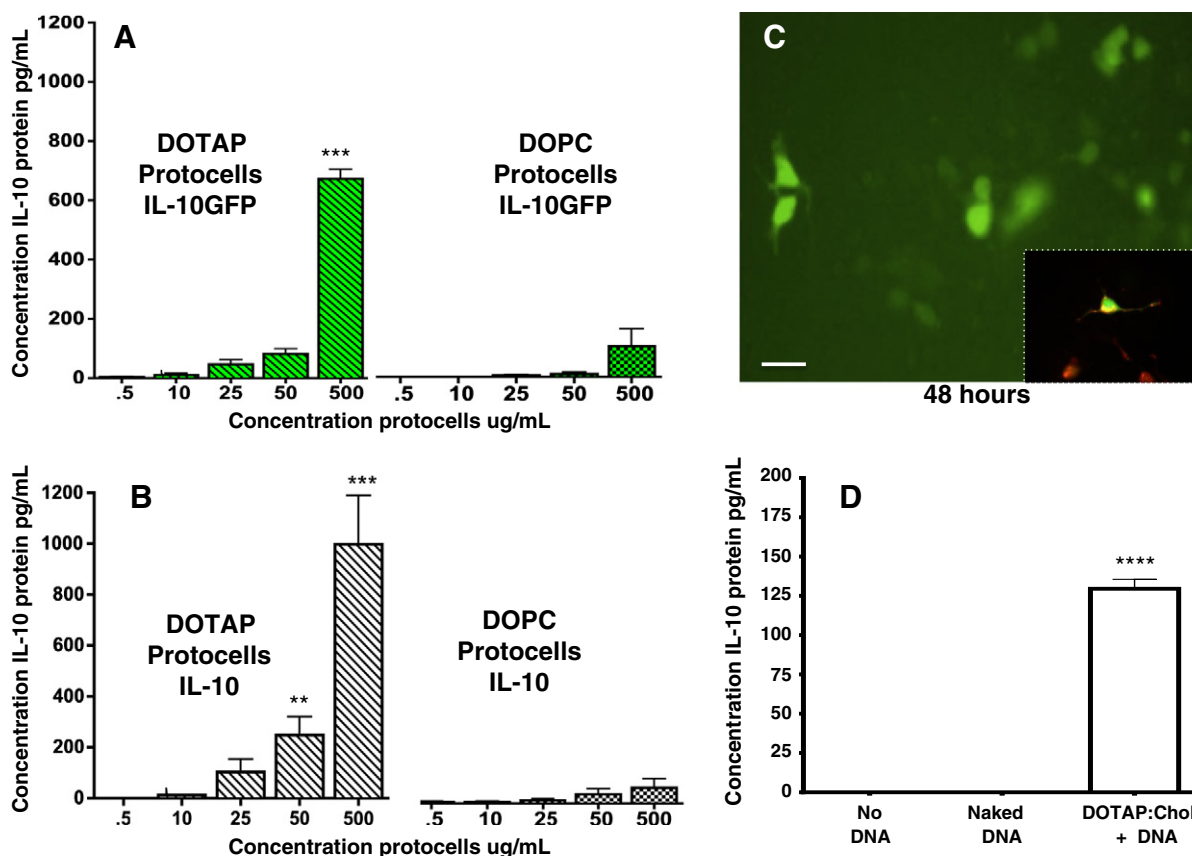


Fig. 6. DOTAP:Chol protocells improve cellular transfection of pDNA-IL10 transgene. (A, C) *In vitro* transfection of HEK cells with a DOTAP:Chol protocells loaded with a bicistronic plasmid containing the genes for both IL-10 and GFP by employing an internal ribosomal entry site, results in expression of both IL-10 and GFP. (B) DOTAP:Chol protocells loaded with pDNA-IL-10 without the GFP transgene and incubated in HEK cells result in robust IL-10 protein. (C; inset) DOTAP:Chol protocells loaded with the bicistronic plasmid, pDNA-IL-10/GFP resulting in functional transgene expression are observed under fluorescent microscopy with GFP-positive HEK cells and staining with antibody for IL-10 (red) reveals colocalization (yellow) ($F_{1,4} = 24.85$; $p < 0.0001$). (D) While DOTAP:Chol liposome without mesoporous silica core results in a significant increase in IL-10 protein expression in pDNA-IL-10 + DOTAP treatment compared to no pDNA-IL-10 and pDNA-IL-10 alone ($F_{(2,9)} = 426.6$; $p < 0.0001$), IL-10 protein levels from DOTAP liposomes + pDNA-IL-10 remain 10-fold less than protein levels resulting from incubation with DOTAP:Chol protocell-pDNA-IL-10 ($p < 0.05$). Secreted recombinant IL-10 from media samples ($N = 4$ /condition) were collected 24 h post-transfection and rat IL-10 protein was quantified using a rat IL-10 specific Quantikine™ ELISA kit. ** $p < 0.01$, *** $p < 0.0001$. Scale bar = 10 µm in both A and inset.

lower levels of IL-10 protein expression (Fig. 6D), suggesting that protocells improve the transfection efficiency of pDNA-IL-10 and that liposomes alone are significantly less efficient.

3.6. Protocells are functionally effective as gene delivery platforms

Given that IL-10 transgene delivered by DOTAP:Chol formulated protocells yielded robust transgene-derived IL-10 protein levels in cell culture (Fig. 6) and DOTAP:Chol protocells appeared to show minimal toxicity *in vivo* (Fig. 3), we next asked whether DOTAP:Chol formulated protocells containing pDNA-IL-10 could act therapeutically by delivering sufficient amounts of the IL-10 transgene to suppress light touch hypersensitivity (allodynia), a neuropathic condition mediated by sensitization of spinal neurons that communicate to brain areas about pain-related stimuli. Allodynia occurs when non-painful stimuli are coded as painful. Following BL assessment of withdrawal behavior to light touch tactile stimuli, rats underwent either sham surgery or CCI of the sciatic nerve. Clear development of allodynia was observed 3 and 10 days later (Fig. 7A, B). On Day 10, rats received an i.t. injection of DOTAP:Chol formulated protocells

containing pDNA-IL-10, pDNA-control (non-coding DNA), or equivalent volume vehicle (20 µl). While sham rats remained stably non-allodynic, a rapid and complete reversal from neuropathic allodynia was observed in IL-10 treated rats. Neuropathic rats injected with i.t. control pDNA or vehicle remained stably allodynic throughout a 26-day timecourse. It is important to note that a prior report demonstrated an equivalent dose of i.t. naked pDNA-IL-10 lacks efficacy to reverse allodynia [12]. Taken together, these data show that pDNA-IL-10 delivered to the peri-spinal regions by DOTAP:Chol protocells was able to reverse allodynia to BL levels for almost 2 weeks. These data support that the production of IL-10 protein from pDNA-IL-10 transgene loaded on protocells is functionally and physiologically effective in reversing pain thresholds.

The toxicity profile of protocells is minimal, as they do not lead to subtle perturbations in cell stress, as assessed by the production of nitric oxide (NO). In order to assess subtle and transient cell-stress responses to the identical DOTAP:Chol protocell formulation examined for *in vivo* spinal gene therapy, cultured macrophage cells (Raw 264.7) were examined, given the observed *in vivo* spinal co-localization of DOTAP:Chol protocells with macrophages/microglial cells, as described above in Fig. 4. Macrophages were assayed for NO following a 2-hour incubation with whole protocells or the component silica core and lipid (DOTAP:Chol) (Fig. 7C). Lipopolysaccharide (LPS) was included, as it is known to produce robust enhancement of NO in this cell line [31–34]. As expected, cells incubated with LPS for 10 min produced increased levels of NO compared to untreated controls. However, similar basal NO levels were observed between untreated controls, whole protocells, silica cores and DOTAP:Chol lipid, suggesting that these materials do not generate transient or even subtle cell stress events.

4. Discussion

Our results demonstrate that mesoporous silica particle cores that support either DOTAP:Chol or DOPC formulated liposomes (protocells) release cargo (Dextran Rhodamine; a negatively charged fluorophore) when exposed to a range of pH values, with greater cargo release occurring at pH 7.4 and higher. Interestingly, protocell cargo is optimally retained at pH 6.0, while lower pH values again induce increased cargo release. Both formulations resulted in high cellular-viability

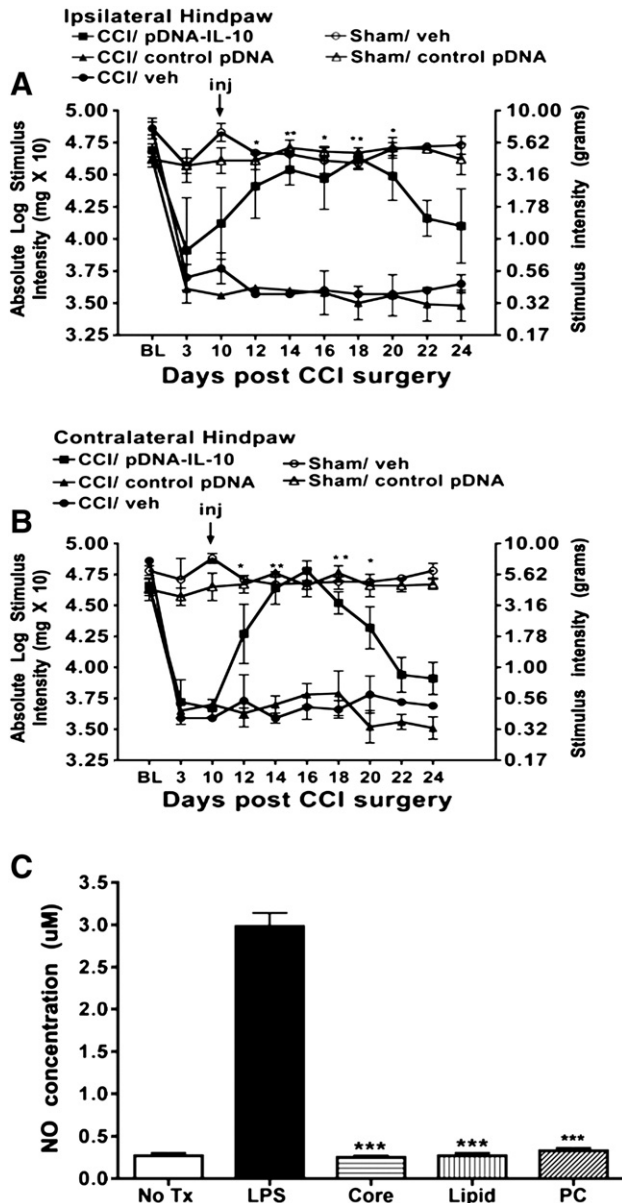


Fig. 7. Intrathecal (i.t.; peri-spinal in direct meningeal contact) delivery of DOTAP:Chol formulated protocells loaded with pDNA-IL-10 causes therapeutic reversal of allodynia. (A and B) At pre-treatment baseline (BL) values, no significant differences were observed in threshold responses of either hindpaw (left and right; $p > 0.05$). Following BL assessment, animals underwent a discrete CCI of the left sciatic nerve to produce neuropathy, and threshold values were reassessed 3 and 10 days later when robust allodynia was observed compared to sham-treated controls (ipsilateral to CCI, $F_{(8,36)} = 4.94$; $p < 0.0004$; contralateral to CCI, $F_{(8,36)} = 19.89$; $p < 0.0001$). On Day 10 after CCI, rats then received an i.t. injection of DOTAP:Chol protocells loaded with pDNA cargo (10 µg) encoding either IL-10 or non-encoding pDNA (as a gene therapy control), or vehicle (20 µl isotonic saline). A significant bilateral reversal of allodynia reached significance on Day 12 after CCI (Day 2 after i.t. injection) that reliably continued through Day 22, with partial reversal observed on Day 24 (ipsilateral hindpaw: $F_{(4,108)} = 44.91$; $p < 0.0001$, contralateral hindpaw: $F_{(4,108)} = 85.09$; $p < 0.0001$). Black squares represent CCI + i.t. pDNA-IL-10 ($n = 7$), black triangles represent non-coding CCI + pDNA ($n = 5$), black circles represent CCI + saline ($n = 3$), open triangles represent sham (no CCI) + i.t. non-coding pDNA ('control pDNA', $n = 5$), and open circles represent sham + vehicle ($n = 3$). Black arrow indicates i.t. injection, 'Inj'; * $p < 0.05$; ** $p < 0.01$; and *** $p < 0.0001$. (C) Nitric oxide (NO) production was assessed to determine cell-stress responses following a 24 hr incubation with DOTAP:Chol protocells loaded with pDNA-IL-10 cargo in the macrophage cell line, Raw 264.7 ($n = 4-5$ wells/condition). LPS, that classically induces cell stress pathways and stimulates NO production (black bar), was used as a positive control. NO levels in cell supernatant from cells without treatment ('No Tx', white bar) to assess background levels of NO, DOTAP:Chol protocells ('PC', hatched bar), or constituents of protocells such as the mesoporous silica core ('Core', 500 µg; horizontal striped bar) or Dotap:Chol lipid ('Lipid', vertical striped bars) were assessed for NO levels. While no significant increase in NO production was observed in cell supernatants following treatment with protocells or its constituents compared to the no treatment controls, LPS treated cells revealed significantly elevated NO levels compared to core, lipid or PC treatment ($F_{(4,14)} = 321.8$; $p < 0.0001$).

values (>90%) following a 50-fold dose range exposure (Figs. 1 and 2). Additionally, peri-spinal application (subarachnoid, intrathecal; i.t.) of either DOTAP:Chol protocells or DOPC formulated protocells in separate groups of rats resulted in minimal sensory changes. Subtle but significant differences in hindpaw sensory threshold values were generally lower in DOPC protocell-treated rats at 2 h compared to thresholds of DOTAP:Chol protocell treated rats (Fig. 3A–D). Importantly, assessment for threshold changes in light mechanical touch from baseline is a sensitive surrogate indicator for physiological spinal cord perturbations involving early-phase inflammatory processes [35] including the generation of nitric oxide (NO) with consequent reactive oxygen species formation and proinflammatory cytokine production (e.g. interleukin-1beta, IL-1 β and tumor necrosis factor-alpha, TNF- α) [19,21,36–39]. The damaging effects of subtle inflammatory processes often go undetected when only employing overt observations for general health measures such as ambulatory function and body weight gain. In studies reported here, an 8-wk observation period for body weight gain revealed no differences between i.t. saline treated and DOTAP:Chol protocell and DOPC protocell-treated animals (Fig. 3E). Spinal immunohistochemical examination of DOTAP:Chol protocells containing DNA revealed clear co-localization with macrophage/microglial cells at the spinal-meningeal interface (Fig. 4D), with a complete lack of cell death, as indicated by the absence of immunoreactivity for the late phase necessary apoptotic enzyme, Caspase-3 (Fig. 4C). Cargo are co-localized with mesoporous silica-

supported DOTAP:Chol liposomes observed 3 days following i.t. protocell injection (Fig. 4H).

While these findings support that DOTAP:Chol protocells offer a significant degree of biocompatibility, clear differences were observed *in vivo* between the biodistribution of DOTAP:Chol formulated and DOPC formulated protocells. Both DOTAP:Chol and DOPC formulated protocell cargo surrounding the spinal cord injection site were identified for as long as 8 weeks following administration (Fig. 5B), but only DOPC protocells revealed an increased spread to brain observed at 8 weeks (Fig. 5A and Table 2). Furthermore, IL-10 transgene expression *in vitro* was significantly greater following cellular incubation with DOTAP:Chol-protocells containing plasmid DNA encoding IL-10 (pDNA-IL-10) than cells incubated with DOPC protocells containing pDNA-IL-10 cargo (Fig. 6A, B). Additionally, DOTAP:Chol protocells revealed superior transfection efficiency to naked pDNA-IL-10 or DOTAP:Chol liposomes alone (Fig. 6D).

Based on the overall profile of DOTAP:Chol protocells as highly biocompatible, localized biodistribution and greater transgene expression, DOTAP:Chol protocells loaded with pDNA-IL-10 cargo were examined for their *in vivo* therapeutic potential as a novel non-viral gene transfer vector delivered to the spinal cord to treat peripheral neuropathic pain. Compared to various control-treated rats, i.t. injections of DOTAP:Chol pDNA-IL-10 protocells resulted in robust reversal of allodynia for as long as 12 days (Fig. 7A, B). Importantly, inflammatory nitric oxide,

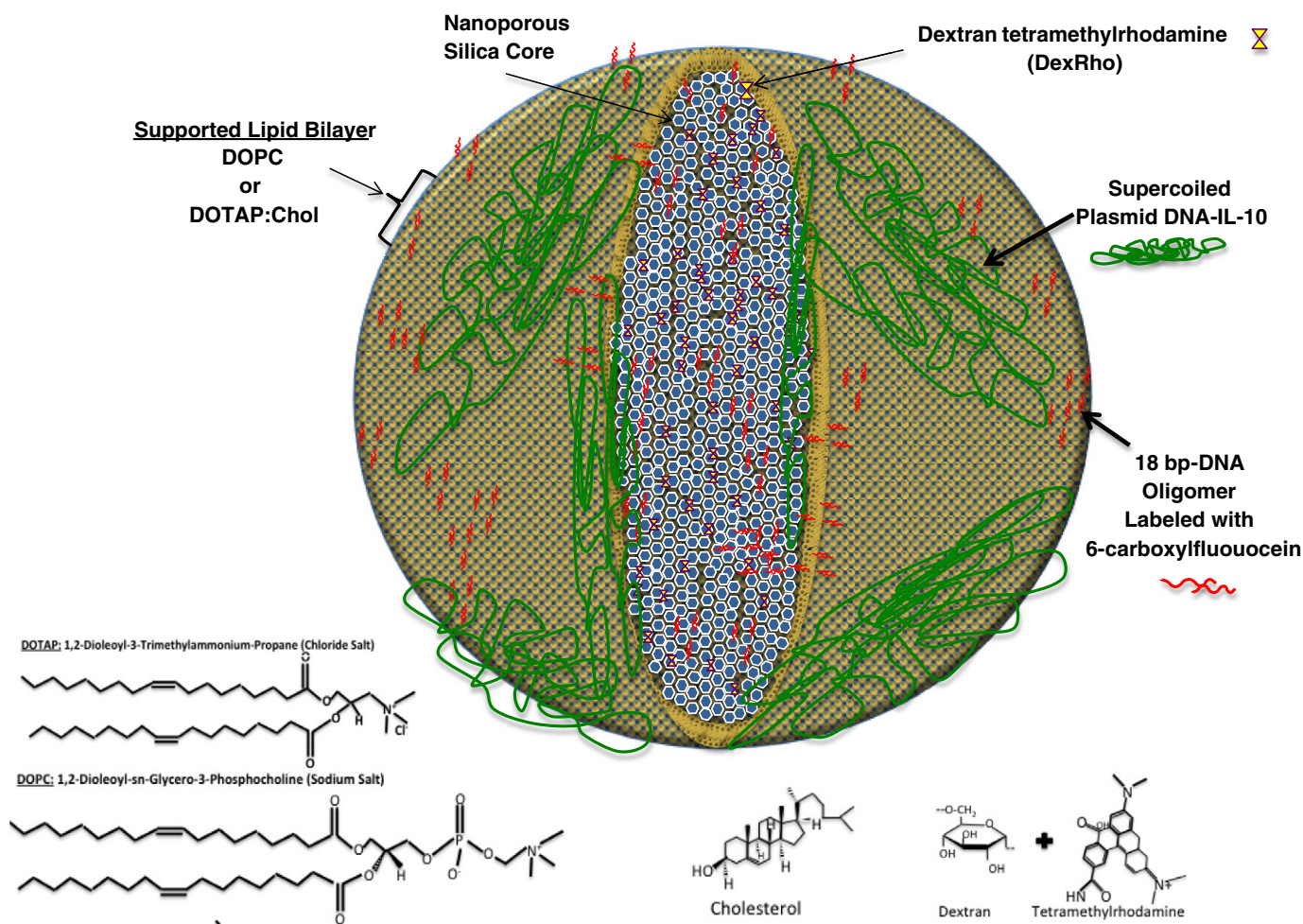


Fig. 8. Schematic representation of the mesoporous silica particle-supported lipid bilayer representing the theoretical loading of the diagnostic molecules and the plasmid DNA-IL-10 gene (pDNA-IL-10) used in this report. The typical 2D hexagonal mesoporous silica is depicted. Supercoiled pDNA-IL-10 (~50 nm) is primarily in between the liposome and at the surface of the protocell, while smaller diagnostic molecules (18-bp DNA and DexRho) load into the silica pores as well as interact with the liposomes. Chemical structures for DOTAP, cholesterol, DOPC and DexRho are provided.

used as a sensitive and specific factor indicative of cell stress, was virtually absent in macrophages exposed to the composite DOTAP:Chol protocell formulation or its constitutive components (Fig. 7C).

A schematic illustration of the mesoporous silica supported lipid bilayer (protocells) showing the theoretical loading characteristics of the diagnostic tools used in these studies (DexRho, 18-bp DNA) or the therapeutic agent, pDNA-IL-10 is shown (Fig. 8). The 5.9 kb pDNA-IL-10 is likely supercoiled and interacts both in between the silica core and the lipid bilayer, but also at the surface of the positively charged DOTAP:Chol lipid bilayer. In future studies, next-generation mesoporous silica cores engineered with ultra large pores are predicted to greatly improve the therapeutic gene delivery as other groups have successfully demonstrated [40,41]. It is important to note that the mesoporous silica cores used in these studies increase loading capacity of small molecules that serve a diagnostic function, or can enhance therapeutic efficacy of drugs or transgene uptake.

The data provided in this report show that protocells are capable of prolonged drug delivery, as DOTAP:Chol-protocells release ~35–40% of negatively charged cargo at pH 7.4, which mimics CSF as well as extracellular pH, during a 1 week timeframe. Protocells at pH 6.0 only release ~25–30% of cargo within a 72 h time frame, which although speculative, may be exploited when increased cargo retention is desired during late endosomal trafficking. Importantly, a substantial amount of protocell cargo content remains for as long as 1 week, supporting the possibility that enduring protocell cargo release for many weeks can be achieved resulting in long-duration therapeutic transgene efficacy. This is particularly desirable for the treatment of chronic CNS diseases such as chronic neuropathic pain. Future studies will determine whether trafficking to late lysosomes containing ~3–4 pH values results in a significant amount of cargo release. While the mechanism of protocell escape from lysosomes remains unknown, pH-dependent cargo release may support an approach that optimizes cargo delivery to specific intracellular compartments with low pH environments. Confocal microscopy shown in the current report demonstrates that protocell cargo is indeed present within and adjacent to cellular nuclei of macrophages in the spinal meninges surrounding the injection site. These observations suggest that while protocells do not necessarily need to enter the nucleus for transgene host cell gene activation, nuclear localization is possible.

While mesoporous silica particles have been widely studied and characterized for *in vitro* biocompatibility, high cargo capacity, tunable pore diameters and surface chemistries [18,42–47], this report is the first *in vivo* demonstration of protocells as non-toxic and functionally capable non-viral spinal gene therapy vectors. The therapeutic application of protocells is highly beneficial for several critical reasons. First, factors indicative of cell stress (nitric oxide; NO) is absent following exposure to whole protocells or the components of protocells (Fig. 7C). Inducible NO is a factor that is rapidly produced following cell stress and inflammation known to mediate the induction of reactive oxygen species further contributing to cell stress [48,49]. Proinflammatory IL-1 β and TNF- α typically contribute to additional NO production, creating ongoing inflammatory processes. Second, the current data also reveal a lack of *in vivo* spinal perturbations (e.g. inflammatory responses) following spinal protocell application (Fig. 3A–D). Indeed, sensory hindpaw response-thresholds remained unchanged from baseline, a physiological 'read-out' of healthy conditions. Third, we further demonstrate that spinal tissue immunohistochemical examination indicated the complete absence of activated Caspase-3 (Fig. 4C), a critical enzyme that mediates programmed cell death [50]. Additionally, we speculate that a large percentage of i.t. protocells escape to the blood circulation where they are cleared by the liver and kidneys with 24h, as protocells or their cargo was absent from peripheral tissues examined at 72 h. Close behavioral assessment, from minutes (30 min), to hours (1, 2, 3, 24 & 72), to weeks (up to 8 weeks) strongly supports a lack of adverse reactivity (normal sensory profiles and weight gain).

Collectively, these properties of protocells make them attractive platforms for non-viral drug or gene delivery using a range of formulations. In the current study, this first-generation protocell supporting a DOTAP:Chol lipid bilayer appears to be functionally effective as spinal gene delivery vehicles for pain-related therapeutic purposes.

The majority of worldwide clinical trials using non-viral gene delivery techniques currently represents ~27% of the total gene therapy clinical trials [51], with these trials mostly applying naked plasmid DNA, and none aimed at neuropathic pain control. However, the examination of gene therapy applications for neuropathic pain in animal models has significantly increased during the past dozen years, with candidate gene products intended to disrupt pain-associated biochemical changes, or themselves, act as analgesics [52]. These trends point to the extraordinary need for new approaches toward developing novel pain therapeutics, as currently available drugs are minimally effective for pathological pain. Thus, the emerging area of CNS gene therapeutics for pain control is rapidly growing.

Neuropathic pain results from pathology in the nervous system and arises from aberrant signals in sensitized injured axons in the peripheral and/or central nervous system [53]. The anti-inflammatory cytokine, IL-10, leads to exceptionally robust suppression of several pain-related conditions including allodynia in various animal models [54]. Allodynia, as assessed in this study, is a pathological sensory condition whereby non-noxious stimuli such as mechanical light touch to the skin are processed as painful [55], and spinal IL-10 gene therapy results in prolonged suppression of chronic allodynia [56]. Indeed, non-viral naked plasmid DNA or polymer-encapsulated gene therapy to control neuropathic pain has been successfully demonstrated in animal models of neuropathic pain [12,13,23]. Interestingly, these non-viral approaches are thought to harness phagocytic innate immune cells that are present at low levels in the peri-spinal meninges and subarachnoid space [12], as an increase in phagocytic macrophages accumulate surrounding the intrathecal lumbar spinal injection site. However, the transgene dose, release rate and cellular targets are constrained by the method of gene delivery used in these prior studies. Conversely, increased transgene dose (cargo retention) and greater flexibility in DNA release rate may be achieved in future-generation protocells used as delivery platforms.

The prior established efficacy of IL-10 for pain control allows comparisons with novel gene delivery approaches, like protocells, that result in therapeutic pain-suppression, and enables one to identify new and improved gene and drug carrier platforms with promising clinical applications. Our data demonstrate that this first-generation DOTAP:Chol protocell formulation is a highly feasible carrier platform for spinal gene therapy. It is important to note that developing next-generation protocell platforms are aimed at delivering cargo that act to stimulate transgene uptake; a multi-therapy approach, and may be superior to existing approaches.

5. Conclusions

This work characterizes the *in vitro* cell stress and *in vivo* physiological profile of liposomes fused on mesoporous silica particles, and examines their use as gene therapeutic vectors delivered to the spinal cord. These liposome-supported mesoporous silica particle constructs are referred to as protocells, which act to retain and protect DNA cargo used in these studies. The advantage of applying protocells as cargo delivery systems (drug and genes) lies not only in their potential for exceptional cargo capacity, but also, as demonstrated in this report, in their high and enduring biocompatibility within the CNS. As non-viral vectors, protocells allow transgenes of interest to remain physiologically functional. Most intriguing is the potential application of this approach to other CNS diseases [57,58] where future-generation protocells can be engineered for cell-specific targeting and tunable release rates. The data in this report demonstrate that protocells loaded with the IL-10 transgene and delivered

peri-spinaly produce robust pain suppression supporting prior reports that spinal IL-10 gene therapy leads to a reduction of pain [12–14,16,23,59,60]. Thus, protocells offer a potentially new drug delivery vessel to the CNS with intrinsic flexibility to tailor drug therapy.

Acknowledgments

The authors would like to thank Linda C. Saland (Department of Neurosciences, University of New Mexico, Albuquerque, New Mexico) for her kind advice regarding tissue immunohistochemistry studies, Becky Lee and Genevieve Phillips (Fluorescence Microscopy Shared Resource, University of New Mexico, Albuquerque, New Mexico) for their assistance in spectral imaging and Tamara Roitbak (Department of Neurosurgery, Health Sciences Center, University of New Mexico) for assisting with confocal imaging. This work was funded by a National Science Foundation IGERT grant: Integrating Nanotechnology with Cell Biology and Neuroscience (DGE 0549500), and a grant from the National Institute on Drug Abuse: #2R01 0181549500.

CJB received support from the NCI Cancer Nanotechnology Platform Partnership grant 1U01CA151792-01; the U.S. Department of Energy, Office of Basic Energy Sciences, Division of Materials Sciences and Engineering; and the Sandia National Laboratories' Laboratory Directed Research and Development (LDRD) program. Sandia is a multiprogram laboratory operated by Sandia Corporation, a wholly owned subsidiary of Lockheed Martin Company, for the US Department of Energy's National Nuclear Security Administration under contract DE-AC04-94AL85000. The authors report no conflict of interest.

References

- [1] M.L. Edelstein, M.R. Abedi, J. Wixon, Gene therapy clinical trials worldwide to 2007—an update, *J Gene Med* 9 (10) (2007) 833–842.
- [2] J. Kaiser, Gene therapists celebrate a decade of progress, *Science* 334 (2011) 29–30.
- [3] F.C. Perez-Martinez, J. Guerra, I. Posadas, V. Cena, Barriers to non-viral vector-mediated gene delivery in the nervous system, *Pharm. Res.* 28 (8) (2011) 1843–1858.
- [4] M. Morille, C. Passirani, A. Vonarbourg, A. Clavreul, J.P. Benoit, Progress in developing cationic vectors for non-viral systemic gene therapy against cancer, *Biomaterials* 29 (24–25) (2008) 3477–3496.
- [5] B.G. Trewyn, S. Giri, Slowing II, V.S. Lin, Mesoporous silica nanoparticle based controlled release, drug delivery, and biosensor systems, *Chem. Commun. (Camb.)* (31) (2007) 3236–3245.
- [6] M.L. Rogers, R.A. Rush, Non-viral gene therapy for neurological diseases, with an emphasis on targeted gene delivery, *J. Control. Release* 157 (2) (2012) 183–189.
- [7] E.J. Park, K. Park, Oxidative stress and pro-inflammatory responses induced by silica nanoparticles in vivo and in vitro, *Toxicol. Lett.* 184 (1) (2009) 18–25.
- [8] S.P. Hudson, R.F. Padera, R. Langer, D.S. Kohane, The biocompatibility of mesoporous silicates, *Biomaterials* 29 (30) (2008) 4045–4055.
- [9] C.E. Ashley, E.C. Carnes, G.K. Phillips, D. Padilla, P.N. Durfee, P.A. Brown, T.N. Hanna, J. Liu, B. Phillips, M.B. Carter, N.J. Carroll, X. Jiang, D.R. Dunphy, C.L. Willman, D.N. Petsev, D.G. Evans, A.N. Parikh, B. Chackerian, W. Wharton, D.S. Peabody, C.J. Brinker, The targeted delivery of multicomponent cargos to cancer cells by nanoporous particle-supported lipid bilayers, *Nat. Mater.* 10 (5) (2011) 389–397.
- [10] D. Tarn, C.E. Ashley, M. Xue, E.C. Carnes, J.I. Zink, C.J. Brinker, Mesoporous Silica Nanoparticle Nanocarriers: Biofunctionality and Biocompatibility, *Acc. Chem. Res.* (2013), <http://dx.doi.org/10.1021/ar3000986>.
- [11] Slowing II, J.L. Vivero-Escoto, C.W. Wu, V.S. Lin, Mesoporous silica nanoparticles as controlled release drug delivery and gene transfection carriers, *Adv. Drug Deliv. Rev.* 60 (11) (2008) 1278–1288.
- [12] E.M. Sloane, S.J. Langer, B.M. Jekich, J.H. Mahoney, T.S. Hughes, W. Seibert, K. Johnson, R.A. Chavez, L.R. Watkins, L.A. Leinwand, E.D. Milligan, Immunological priming potentiates non-viral anti-inflammatory gene therapy treatment of neuropathic pain, *Gene Ther.* 1 (2009) 1–13.
- [13] R.G. Soderquist, E.M. Sloane, L.C. Loram, J.A. Harrison, E.C. Dengler, S.M. Johnson, L.D. Amer, C.S. Young, M.T. Lewis, S. Poole, M.G. Frank, L.R. Watkins, E.D. Milligan, M.J. Mahoney, Release of plasmid DNA-encoding IL-10 from PLGA microparticles facilitates long-term reversal of neuropathic pain following a single intrathecal administration, *Pharm. Res.* 27 (5) (2010) 841–854.
- [14] E.D. Milligan, S.J. Langer, E.M. Sloane, L. He, J. Wieseler-Frank, K.A. O'Connor, D. Martin, J.R. Forsayeth, S.F. Maier, K. Johnson, R.A. Chavez, L.A. Leinwand, L.R. Watkins, Controlling pathological pain by adenovirally driven spinal production of the anti-inflammatory cytokine, Interleukin-10, *Eur. J. Neurosci.* 21 (2005) 2136–2148.
- [15] A.S. Beutler, M.S. Banck, C.E. Walsh, E.D. Milligan, Intrathecal gene transfer by adeno-associated virus for pain, *Curr. Opin. Mol. Ther.* 7 (5) (2005) 431–439.
- [16] E.D. Milligan, R.G. Soderquist, S.M. Malone, J.H. Mahoney, T.S. Hughes, S.J. Langer, E.M. Sloane, S.F. Maier, L.A. Leinwand, L.R. Watkins, M.J. Mahoney, Intrathecal polymer-based interleukin-10⁺ gene delivery for neuropathic pain, *Neuron Glia Biol.* 2 (2006) 293–308.
- [17] J. Liu, X. Jiang, C. Ashley, C.J. Brinker, Electrostatically mediated liposome fusion and lipid exchange with a nanoparticle-supported bilayer for control of surface charge, drug containment, and delivery, *J. Am. Chem. Soc.* 131 (22) (2009) 7567–7569.
- [18] J. Liu, A. Stace-Naughton, X. Jiang, C.J. Brinker, Porous nanoparticle supported lipid bilayers (protocells) as delivery vehicles, *J. Am. Chem. Soc.* 131 (4) (2009) 1354–1355.
- [19] S.R. Chaplan, F.W. Bach, J.W. Pogrel, J.M. Chung, T.L. Yaksh, Quantitative assessment of tactile allodynia in the rat paw, *J. Neurosci. Methods* 53 (1994) 55–63.
- [20] E.D. Milligan, K.K. Mehmert, J.L. Hinde, L.O.J. Harvey, D. Martin, K.J. Tracey, S.F. Maier, L.R. Watkins, Thermal hyperalgesia and mechanical allodynia produced by intrathecal administration of the Human Immunodeficiency Virus-1 (HIV-1) envelope glycoprotein, gp120, *Brain Res.* 861 (2000) 105–116.
- [21] E.D. Milligan, K.A. O'Connor, K.T. Nguyen, C.B. Armstrong, C. Twining, R. Gaykema, A. Holguin, D. Martin, S.F. Maier, L.R. Watkins, Intrathecal HIV-1 envelope glycoprotein gp120 enhanced pain states mediated by spinal cord proinflammatory cytokines, *J. Neurosci.* 21 (2001) 2808–2819.
- [22] G.J. Bennett, K.Y. Xie, A peripheral mononeuropathy in rat that produces disorders of pain sensation like those seen in man, *Pain* 33 (1988) 87–107.
- [23] E.D. Milligan, E.M. Sloane, S.J. Langer, T.R. Hughes, B.M. Jekich, M.G. Frank, J.H. Mahoney, L.H. Levkoff, S.F. Maier, P.E. Cruz, T.R. Flotte, K.W. Johnson, M.M. Mahoney, R.A. Chavez, L.A. Leinwand, L.R. Watkins, Repeated intrathecal injections of plasmid DNA encoding interleukin-10 produce prolonged reversal of neuropathic pain, *Pain* 126 (2006) 294–308.
- [24] R. Langer, Drug delivery and targeting, *Nature* 392 (6679 Suppl.) (1998) 5–10.
- [25] K. Crook, B.J. Stevenson, M. Dubouchet, D.J. Porteous, Inclusion of cholesterol in DOTAP transfection complexes increases the delivery of DNA to cells in vitro in the presence of serum, *Gene Ther.* 5 (1) (1998) 137–143.
- [26] E. Barrett, L. Joyner, P. Halenda, The Determination of Pore volume and Area distributions in Porous Substances. I. Computations from Nitrogen isotherms, *J. Am. Chem. Soc.* 73 (1) (1951) 373–380.
- [27] X. Jiang, C.J. Brinker, Aerosol-assisted self-assembly of single-crystal core/nanoporous shell particles as model controlled release capsules, *J. Am. Chem. Soc.* 128 (14) (2006) 4512–4513.
- [28] S. Brunauer, P. Emmett, E. Teller, Adsorption of Gases in Multimolecular Layers, *J. Am. Chem. Soc.* 60 (2) (1938) 309–319.
- [29] J.L. Wilkerson, K.R. Gentry, E.C. Dengler, J.A. Wallace, A.A. Kerwin, M.N. Kuhn, A.M. Zvonok, G.A. Thakur, A. Makriyannis, E.D. Milligan, Immunofluorescent spectral analysis reveals the intrathecal cannabinoid agonist, AM1241, produces spinal anti-inflammatory cytokine responses in neuropathic rats exhibiting relief from allodynia, *Brain Behav.* 2 (2) (2012) 155–177.
- [30] L.O.J. Harvey, Efficient estimation of sensory thresholds, *Behav. Res. Methods Instrum. Comput.* 18 (1986) 623–632.
- [31] A. Khan, et al., Sustained polymeric delivery of gene silencing antisense ODNs, siRNA, DNazymes and ribozymes: in vitro and in vivo studies, *J. Drug Target.* 12 (6) (2004) 393–404.
- [32] J.K. Lee, Anti-inflammatory effects of eriodictyol in lipopolysaccharide-stimulated raw 264.7 murine macrophages, *Arch. Pharm. Res.* 34 (4) (2011) 671–679.
- [33] A.A. Qureshi, X. Tan, J.C. Reis, M.Z. Badr, C.J. Papisian, D.C. Morrison, N. Qureshi, Suppression of nitric oxide induction and pro-inflammatory cytokines by novel peptosome inhibitors in various experimental models, *Lipids Health Dis.* 10 (2011) 177.
- [34] L.Y. Zha, L.M. Mao, X.C. Lu, H. Deng, J.F. Ye, X.W. Chu, S.X. Sun, H.J. Luo, Anti-inflammatory effect of soyasaponins through suppressing nitric oxide production in LPS-stimulated RAW 264.7 cells by attenuation of NF- κ B-mediated nitric oxide synthesis expression, *Bioorg. Med. Chem. Lett.* 21 (8) (2011) 2415–2418.
- [35] Y. Kawasaki, L. Zhang, J.-K. Cheng, R.-R. Ji, Cytokine mechanisms of central sensitization: Distinct and overlapping role of interleukin-1 β , interleukin-6, and tumor necrosis factor- α in regulating synaptic and neuronal activity in the superficial spinal cord, *J. Neurosci.* 28 (20) (2008) 5189–5194.
- [36] T.A. Samad, K.A. Moore, A. Sapirstein, S. Billet, A. Allchorne, S. Poole, J.V. Bonventre, Interleukin-1 β -mediated induction of COX-2 in the CNS contributes to inflammatory pain hypersensitivity, *Nature* 410 (2001) 471–475.
- [37] T.A. Samad, H. Wang, D.C. Broom, C.J. Woolf, Central neuroimmune interactions after peripheral inflammation: interleukin-1 β potentiates synaptic transmission in the spinal cord, *Proc Soc Neurosci.* 2004.
- [38] M.E. Smith, K. van der Maesen, F.P. Somera, Macrophage and microglial responses to cytokines in vitro: phagocytic activity, proteolytic enzyme release, and free radical production, *J. Neurosci. Res.* 54 (1) (1998) 68–78.
- [39] L.R. Watkins, S.F. Maier, Beyond neurons: evidence that immune and glial cells contribute to pathological pain states, *Physiol. Rev.* 82 (4) (2002) 981–1011.
- [40] F. Gao, P. Botella, A. Corma, J. Blesa, L. Dong, Monodispersed mesoporous silica nanoparticles with very large pores for enhanced adsorption and release of DNA, *J. Phys. Chem. B* 113 (6) (2009) 1796–1804.
- [41] M.H. Kim, H.K. Na, Y.K. Kim, S.R. Ryoo, H.S. Cho, K.E. Lee, H. Jeon, R. Ryoo, D.H. Min, Facile synthesis of monodispersed mesoporous silica nanoparticles with ultralarge pores and their application in gene delivery, *ACS Nano* 5 (5) (2011) 3568–3576.
- [42] L.M. Bimbo, L. Peltonen, J. Hirvonen, H.A. Santos, Toxicological profile of therapeutic nanodelivery systems, *Curr. Drug Metab.* 13 (8) (2012) 1068–1086.
- [43] R.W. Davis, A. Flores, T.A. Barrick, J.M. Cox, S.M. Brozik, G.P. Lopez, J.A. Brozik, Nanoporous microbead supported bilayers: stability, physical characterization,

- and incorporation of functional transmembrane proteins, *Langmuir* 23 (7) (2007) 3864–3872.
- [44] E. Sackmann, Supported membranes: scientific and practical applications, *Science* 271 (5245) (1996) 43–48.
- [45] K.P. Singh, P. Panwar, P. Kohli, Sanjesh, Liposome-mesoporous silica nanoparticles fused cores: a safer mode of drug carrier, *J. Biomed. Nanotechnol.* 7 (1) (2011) 60–62.
- [46] A.L. Troutier, C. Ladaviere, An overview of lipid membrane supported by colloidal particles, *Adv. Colloid Interf. Sci.* 133 (1) (2007) 1–21.
- [47] T.H. Yang, C.K. Yee, M.L. Amweg, S. Singh, E.L. Kendall, A.M. Dattelbaum, A.P. Shreve, C.J. Brinker, A.N. Parikh, Optical detection of ion-channel-induced proton transport in supported phospholipid bilayers, *Nano Lett.* 7 (8) (2007) 2446–2451.
- [48] Y. Son, Y.K. Cheong, N.H. Kim, H.T. Chung, D.G. Kang, H.O. Pae, Mitogen-Activated Protein Kinases and Reactive Oxygen Species: How Can ROS Activate MAPK Pathways? *J. Signal Transduct.* 2011 (2011) 792639.
- [49] S. Murphy, D. Grzybycki, Glial NO: Normal and pathological roles, *Neuroscientist* 2 (2) (1996) 90–99.
- [50] X. Wang, C. Wang, J. Zeng, X. Xu, P.Y. Hwang, W.C. Yee, Y.K. Ng, S. Wang, Gene transfer to dorsal root ganglia by intrathecal injection: effects on regeneration of peripheral nerves, *Mol. Ther.* 12 (2) (2005) 314–320.
- [51] S.L. Ginn, I.E. Alexander, M.L. Edelstein, M.R. Abedi, J. Wixon, Gene therapy clinical trials worldwide to 2012 - an update, *J. Gene Med.* 15 (2) (2013) 65–77.
- [52] J.R. Goss, W.F. Goins, J.C. Glorioso, Gene therapy applications for the treatment of neuropathic pain, *Expert Rev. Neurother.* 7 (5) (2007) 487–506.
- [53] J.N. Campbell, R.A. Meyer, Mechanism of neuropathic pain, *Neuron* 52 (2006) 77–92.
- [54] E.D. Milligan, K.R. Penzkover, R.G. Soderquist, M.J. Mahoney, Spinal interleukin-10 therapy to treat peripheral neuropathic pain, *Neuromodulation* 15 (6) (2012) 520–526.
- [55] L.S. Miracourt, R. Dallel, D.L. Voisin, Glycine inhibitory dysfunction turns touch into pain through PKCgamma interneurons, *PLoS One* 2 (11) (2007) e1116.
- [56] E.M. Sloane, R.G. Soderquist, S.F. Maier, M.J. Mahoney, L.R. Watkins, E.D. Milligan, Long-term control of neuropathic pain in a non-viral gene therapy paradigm, *Gene Ther.* 16 (4) (2009) 470–475.
- [57] D.J. Bharali, I. Klejbor, E.K. Stachowiak, P. Dutta, I. Roy, N. Kaur, E.J. Bergey, P.N. Prasad, M.K. Stachowiak, Organically modified silica nanoparticles: a nonviral vector for in vivo gene delivery and expression in the brain, *Proc. Natl. Acad. Sci. U. S. A.* 102 (32) (2005) 11539–11544.
- [58] I. Roy, T.Y. Ohulchanskyy, D.J. Bharali, H.E. Pudavar, R.A. Mistretta, N. Kaur, P.N. Prasad, Optical tracking of organically modified silica nanoparticles as DNA carriers: a nonviral, nanomedicine approach for gene delivery, *Proc. Natl. Acad. Sci. U. S. A.* 102 (2) (2005) 279–284.
- [59] A. Ledebuer, E.M. Sloane, E.D. Milligan, S.J. Langer, S.F. Maier, K.W. Johnson, L.A. Leinwand, R.A. Chavez, L.R. Watkins, Paclitaxel-induced mechanical allodynia in rats is inhibited by spinal delivery of plasmid DNA encoding interleukin-10, *Proceedings of the 11th World Congress on Pain, International Association for the Study of Pain, Sydney, Australia, 2006.*
- [60] E.D. Milligan, E.M. Sloane, S.J. Langer, P.E. Cruz, M. Chacur, L. Spataro, J. Wieseler-Frank, S.E. Hammack, S.F. Maier, T.R. Flotte, J.R. Forsayeth, L.A. Leinwand, R.A. Chavez, L.R. Watkins, Controlling neuropathic pain by adeno-associated virus driven production of the anti-inflammatory cytokine, interleukin-10, *Mol. Pain* 1 (2005) 9–22.